People's Democratic Republic of Algeria

Ministry of Higher Education and

Scientific Research

Echahid Hamma Lakhdar University of El-Oued

Faculty of Technology Major: Electrical Engineering

End of study dissertation

Presented for graduation from

ACADEMIC MASTERS

In: Telecommunication

Specialty: Telecommunication systems

By: Hachachen Abir, Dridi Nadjoua

Theme

Simulation Study of Bilayer Absorber Perovskite Solar Cells Using SCAPS-1D

In front of the jury composed of:

Mr. Aouragh Nabil	**University Echahid Hamma Lakhdar**	**President**
Mr. Hima Abdelkader	**University Echahid Hamma Lakhdar**	**Examinator**
Mr. Tinedert Imad Eddine	**University Echahid Hamma Lakhdar**	**Supervisor**

2023-2024

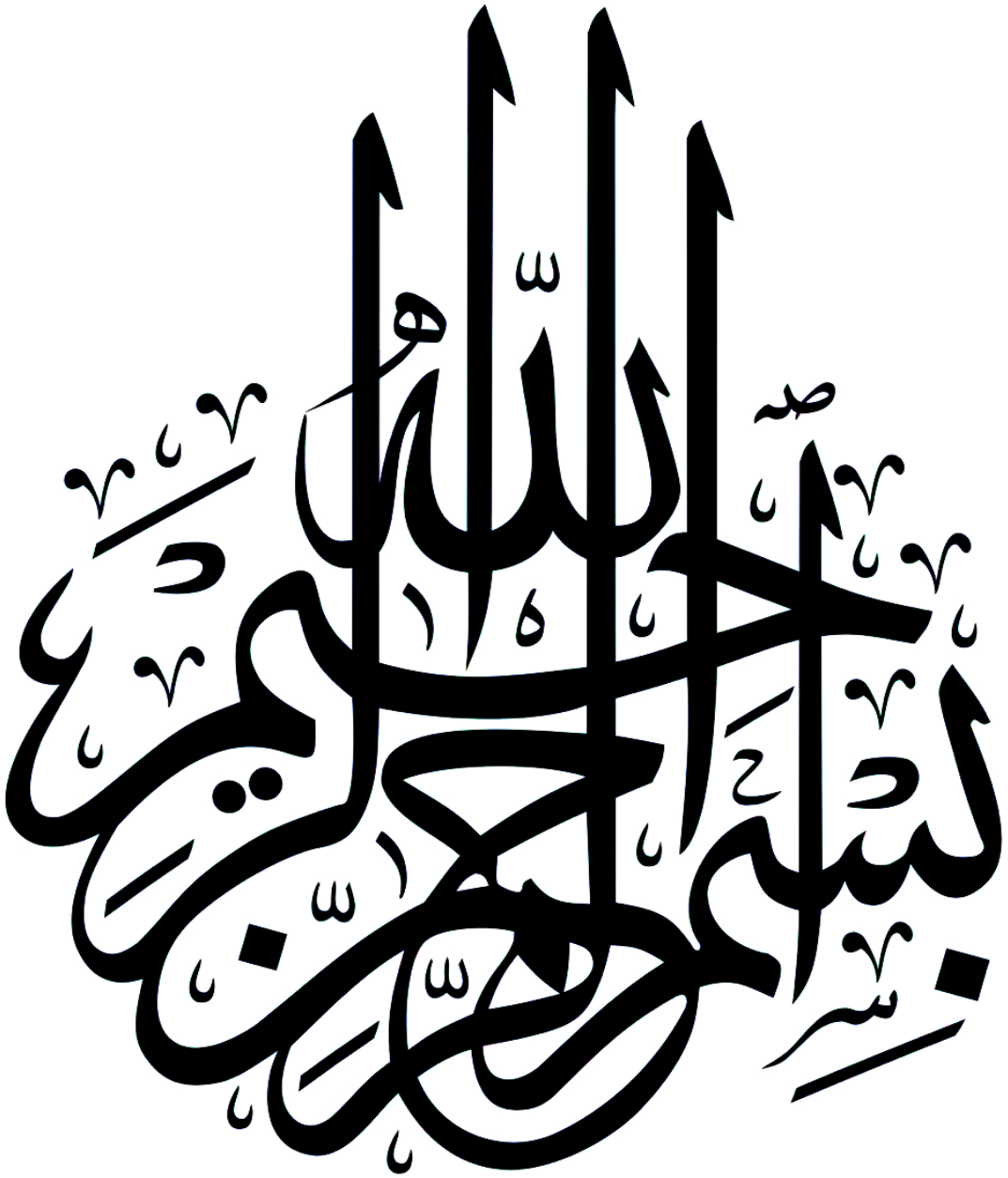
بسم الله الرحمن الرحيم

Acknowledgements

First and foremost, we extend our deepest gratitude to Allah, whose boundless mercy and grace have guided us through every step of this journey. With hearts full of thankfulness, we acknowledge His divine wisdom, which has served as a guiding light in moments of uncertainty, and His unwavering strength, which has carried us through seemingly insurmountable challenges.

We thank Allah for the clarity of mind, perseverance, and inspiration that have accompanied us throughout the writing of this thesis. It is by His blessings that we have been able to overcome every obstacle, and we see His hand in every success, feeling His presence in every moment of accomplishment. To Allah be the glory for the completion of this work, and may His blessings continue to illuminate our future endeavors.

We would also like to express our heartfelt thanks to our families, whose unwavering support and encouragement have been invaluable throughout this journey. Their love and belief in us have been a constant source of motivation. Additionally, we extend our sincere gratitude to our professors, whose guidance, wisdom, and encouragement have been instrumental in shaping this thesis. Their dedication to our education and growth has been a cornerstone of our academic journey, and for that, we are deeply grateful.

Dedication

As I come to the end of this academic journey, I find myself filled with profound gratitude to the many individuals who have supported me along the way.

First and foremost, I would like to express my deepest gratitude to my family, whose unwavering love and encouragement have been the cornerstone of my perseverance. **To my parents**, I am deeply grateful for their endless patience, belief in my potential, and the countless sacrifices you have made to help me get to this point. **To my siblings**, your companionship and understanding have lightened my burdens; your presence has been a constant source of strength. Thank you for your sense of humor and kindness, and for always reminding me of the joy that can be found even in the most difficult times.

I am also deeply grateful **to my supervisor, Dr. Tinedert Imad Eddine**. Her expertise and passion for knowledge have inspired me to strive for excellence.

Finally, I would like to thank my friends and colleagues for the companionship, study sessions, and shared experiences that have made this journey unforgettable. I am proud to have walked this path alongside you.

This thesis is the result of a team effort, and I am deeply grateful to everyone who participated in this journey.

This achievement is due to all of you.

With all my love and appreciation.

Hachachen Abir

Dedication

Praise be to Allah, in love, gratitude, and thankfulness, for the beginning and the end.

First, we thank Almighty Allah for granting us the strength needed to accomplish this work.

To the symbol of giving and sacrifice,

my dear father

To the one who greets me with a smile and bids me farewell with prayers,

my dear mother

To that great repository of strength and love,

my brothers and sisters

To my supervisor, Dr. Tinedert Imad Eddine, *who guided us to accomplish this work with his invaluable advice and assistance.*

We would also like to thank the head of the committee and the esteemed professors on the panel.

With all my love and appreciation.

Dridi Nadjoua

ملخص

في السنوات الاخيرة عرفت الخلايا الشمسية القائمة على بيروفسكايت تطور كبير و إهتمام واسع بسبب الكفاءة العالية والاستقرار في الاداء لهذا النوع. في هذه المذكرة تم دراسة الخلية الشمسية بيروفسكايت ثنائية الطبقة الماصة $CsPbIBr_2/KsnI_3$ بواسطة محاكاة رقمية باستخدام برنامج المحاكاة SCAPS-1D .

في الخطوة الاولى من هذا العمل تمت دراسة ومحاكاة هيكل مرجعي للخلية الشمسية $FTO/SnO_2/CsPbIBr_2/Spiro/Au$ وذلك للتحقق من صحة المحاكاة وتوافق النتائج المتحصل عليها مع البيانات التجريبية. تحصلنا على مردود يقدر ب 9.70% وهاته النتيجة تتوافق بشكل كبير مع الخلايا التجريبية.

من أجل الرفع من كفاءة الخلية تم اضافة مادة ماصة جديدة $KsnI_3$ بمثابة طبقة ماصة سفلية والتي تساهم في توسيع نطاق الامتصاص للخلية ليصبح الهيكل الجديد من الشكل $FTO/SnO_2/CsPbIBr_2/KsnI_3/Spiro/Au$ وقد ساهمت هذه الاضافة في رفع الكفاءة بشكل كبير مقارنة بالهيكل الأول الذي يعتمد على طبقة ماصة واحدة حيث أصبح مردود الخلية يقارب 16.9% .

في الخطوة التالية قمنا بدراسة تأثير بعض المعلمات الأساسية مثل السمك وتركيز التطعيم للمادتين الماصتين وذلك من أجل تحسين الهيكل القائم عن الطبقتين الماصتين $CsPbIBr_2/KsnI_3$.

أحسن مردود تم الحصول عليه هو 19.89 % وذلك من اجل سمك 700 و 1000 نانومتر و كذلك بتركيز $1 \times 10^{16}\ cm^{-3}$ و $1 \times 10^{15}\ cm^{-3}$ لثنائي الطبقة الماصة $CsPbIBr_2/KSnI_3$ علي الترتيب.

واخيرا درسنا تأثير درجة الحرارة على كفاءة الخلية الشمسية المحسنة في المجال المحصور من 260 -350 كلفن وقد بينت نتائج المحاكاة ان الكفاءة تنخفض عند درجات الحرارة العالية جدا.

الكلمات المفتاحية: ممتص ثنائي الطبقة، خلية بيروفسكايت الشمسية، فجوة نطاق واسعة، $CsPbIBr_2$، PCE، SCAPS-1D.

Abstract

In recent years, perovskite-based solar cells have seen significant development and widespread interest due to their high efficiency and stable performance. In this thesis, the $CsPbIBr_2/KSnI_3$ bilayer perovskite solar cell was studied through numerical simulation using the SCAPS-1D simulation program.

In the first step of this work, the reference structure of the solar cell $FTO/SnO_2/CsPbIBr_2/Spiro/Au$ was studied and simulated to verify the accuracy of the simulation and the compatibility of the obtained results with experimental data. We achieved an efficiency of 9.70%, which is highly consistent with experimental cells.

To enhance the cell's efficiency, a new absorber material, KSnI3, was added as a bottom absorber layer, contributing to the broadening of the cell's absorption range. This resulted in the new structure $FTO/SnO_2/CsPbIBr_2/KSnI_3/Spiro/Au$, which significantly increased the efficiency compared to the first structure that relies on a single absorber layer, with the cell efficiency reaching approximately 16.9%.

In the next step, we studied the effect of some key parameters such as the thickness and doping concentration of the two absorbers to improve the $CsPbIBr_2/KSnI_3$ bilayer perovskite solar cell. The best efficiency obtained was a PCE of 19.89% for thicknesses of 700 and 1000 nanometers and doping concentrations of $1x10^{15}$ and $1x10^{16}$ cm^{-3} for the dual absorber layers $CsPbIBr_2$ and $KSnI_3$, respectively.

Finally, we studied the effect of temperature on the efficiency of the optimized solar cell within the range of 260-350 Kelvin. The simulation results showed that efficiency decreases at very high temperatures.

Keywords: Bilayer absorber, Perovskite solar cell, Wide bandgap, $CsPbIBr_2$, PCE, SCAPS-1D.

Résumé

Ces dernières années, les cellules solaires à base de pérovskites ont connu un développement significatif et suscité un intérêt considérable en raison de leur haute efficacité et de leurs performances stables. Dans cette thèse, la cellule solaire à pérovskite bicouche $CsPbIBr_2/KSnI_3$ a été étudiée par simulation numérique en utilisant le programme de simulation SCAPS-1D.

Dans la première étape de ce travail, la structure de référence de la cellule solaire $FTO/SnO_2/CsPbIBr_2/Spiro/Au$ a été étudiée et simulée afin de vérifier l'exactitude de la simulation et la compatibilité des résultats obtenus avec les données expérimentales. Nous avons obtenu une efficacité de 9,70%, ce qui est très cohérent avec les cellules expérimentales.

Pour améliorer l'efficacité de la cellule, un nouveau matériau absorbeur, le $KSnI_3$, a été ajouté en tant que couche absorbante inférieure, contribuant à élargir la gamme d'absorption de la cellule. Cela a abouti à la nouvelle structure $FTO/SnO_2/CsPbIBr_2/KSnI_3/Spiro/Au$, qui a significativement augmenté l'efficacité par rapport à la première structure reposant sur une seule couche absorbante, l'efficacité de la cellule atteignant environ 16,9%.

Dans l'étape suivante, nous avons étudié l'effet de certains paramètres clés tels que l'épaisseur et la concentration de dopage des deux absorbeurs pour améliorer la cellule solaire à pérovskite bicouche $CsPbIBr_2/KSnI_3$. La meilleure efficacité obtenue était une PCE de 19,89% pour des épaisseurs de 700 et 1000 nanomètres et des concentrations de dopage de $1x10^{15}$ and $1x10^{16}$ cm^{-3} pour les couches absorbantes $CsPbIBr_2$ et $KSnI_3$, respectivement.

Enfin, nous avons étudié l'effet de la température sur l'efficacité de la cellule solaire optimisée dans une plage de 260 à 350 Kelvin. Les résultats de la simulation ont montré que l'efficacité diminue à des températures très élevées.

Mots clés : Absorbeur bicouche, Cellule solaire pérovskite, $CsPbIBr_2$, PCE, SCAPS-1D.

Table of contents

List of figures

List of tables

General Introduction

General Introduction

Solar cells are a vital technology for converting solar energy into electrical energy, representing one of the most prominent applications of renewable energy in the modern era. The discovery of solar cells dates back to the 19th century when French physicist Alexandre Edmond Becquerel directed sunlight onto electrical cells and found that they generated an electric current. Since then, solar cell technology has seen continuous development. Solar cells vary in type based on the materials used in their manufacture, including crystalline silicon solar cells, composite cells, organic solar cells, and perovskite cells. The working principle of a solar cell is based on the conversion of light energy into electrical energy through the photoelectric effect, where an electron-hole pair is generated when photons are absorbed.

Perovskite solar cells (PSCs) are an innovative and rapidly advancing technology in the field of photovoltaic energy conversion. Named after the perovskite-structured material used as the light-harvesting active layer, these solar cells have garnered significant attention due to their remarkable efficiency and potential for low-cost production. The perovskite material, typically a hybrid of organic and inorganic compounds, possesses excellent light absorption properties. These characteristics enable PSCs to convert sunlight into electricity with high efficiency, making them one of the most promising alternatives to traditional silicon-based solar cells.

The performance of solar cells is evaluated using various parameters such as open circuit voltage (Voc), short circuit current (Isc), fill factor (FF), and power conversion efficiency (PCE)

Recent research has shown significant improvements in solar cell efficiency, with perovskite solar cell efficiency reaching 26%, reflecting continued progress in this vital field.

Despite improvements in single-junction solar cell efficiency, they are still limited by the Shockley-Queisser limit and thermodynamic constraints. The most effective method to surpass this limit is by using bilayer or multilayer heterojunction structures. In a bilayer heterojunction, two different perovskite materials with varying bandgaps are layered, allowing for a broader absorption of the sunlight spectrum. This configuration enhances photogenerated carrier production, leading to higher PCE.

This thesis focuses on the study and optimization of $CsPbIBr_2/KSnI_3$ bilayer perovskite solar cells (PSCs) through numerical simulation using the SCAPS-1D simulation program. After validating our simulation of a single junction based on $CsPbIBr_2$ with previously reported

experimental results in the literature, we compare the performance with that of $CsPbIBr_2/KSnI_3$ bilayer PSCs. In the second part, we aim to improve the $CsPbIBr_2/KSnI_3$ bilayer PSCs in terms of thickness, doping density, and other parameters.

This thesis is divided into three chapters organized as follows:

- ✓ **Chapter 1:** This chapter includes background information on solar radiation and the photovoltaic effect, semiconductors and p-n junctions, solar cell fundamentals and their operation, and solar cell loss processes. This chapter concludes with a presentation of the many kinds of solar cells and the most recent findings.

- ✓ **Chapter 2:** The second chapter focuses on perovskite solar cells, detailing the compounds commonly used in their manufacture. Special attention is given to the characteristics and materials utilized in our work, including materials that transmit solar radiation (such as FTO and SnO_2) and those that absorb photons, namely all-inorganic $CsPbIBr_2$ and $KsnI_3$ perovskites. Additionally, the SCAPS-1D simulation program, along with its key commands and the fundamental equations necessary for successful simulation, will be thoroughly explained.

- ✓ **Chapter 3:** This chapter presents a comparison and validation of the simulated cell with experimental cells, specifically the $FTO/SnO_2/CsPbIBr_2/Spiro/Au$ structure. To improve the cell's performance, we proposed adding a new material to create a bilayer PSC, forming the $FTO/SnO_2/CsPbIBr_2/KSnI_3/Spiro/Au$ structure. Although we observed an increase in efficiency after the addition of the new material, further optimization of the bilayer absorber, in terms of thickness and doping density, was performed to achieve optimal efficiency. Finally, we examine how the efficiency of solar cells varies with temperature.

Chapter 1: Basics of photovoltaic cells

1.1.Introduction

The solar cell is a transformative technology that converts solar energy into electrical energy, representing one of the most significant advancements in renewable energy. The origins of the solar cell trace back to the nineteenth century, when French physicist Alexandre Edmond Becquerel observed that directing sunlight onto electrical cells generated an electric current. Since Becquerel's pioneering discovery, solar cell technology has undergone continuous innovation and development. Today, various types of solar cells exist, differentiated by the materials used in their production. These include coaxial silicon solar cells, composite solar cells, organic solar cells, and the more recent perovskite solar cells. The fundamental operation of a solar cell relies on the photovoltaic effect, where the absorption of photons generates an electronic gap and an electronic hole, effectively converting light energy into electrical energy. Key performance metrics of solar cells include open circuit voltage (V_{oc}), short circuit current (I_{sc}), maximum power point (Pm), fill factor (FF), and overall efficiency (η). As solar cell technology advances, it holds the promise of playing a crucial role in the global transition to sustainable energy sources.

In this chapter, we introduce fundamental concepts of the p-n junction and the photovoltaic effect, which form the foundation of nearly all photovoltaic devices. These basics are essential for understanding the operation of solar cells and the conversion of sunlight into electricity. We then present equivalent circuit diagrams of solar cells and discuss their essential performance characteristics and calculation methods. Additionally, we explore the loss mechanisms in solar cells. Finally, we review various types of solar cells and highlight the highest confirmed conversion efficiencies to date.

1.2.Solar radiation

It is the energy emitted by the sun in the form of electromagnetic radiation. This radiation includes a wide range of wavelengths, including visible light, ultraviolet light, and infrared light. Solar radiation reaches the Earth and is the primary source of thermal and light energy that supports life and affects climate and weather processes [13].

1.2.1. Air Mass

The electromagnetic radiation emitted by the sun outside Earth's atmosphere is referred to as AM 0 (Air Mass 0). In contrast, AM 1 indicates that the light has passed through the atmosphere, as illustrated in Figure 1.1. Additionally, according to Planck's Law of Radiation, AM 0 represents radiation emitted by a black body (the sun's surface at a temperature of 5778 K, as shown in Figure 1.1). The radiation's path through the atmosphere ($1/\cos\theta$), combined with natural factors (Figure

1.1), influences the light, resulting in the AM x spectrum, depicted in Figure 1.2, where (x = 1, … ,4). The area under the AM 1.5 curve, corresponding to (1/cos 48°), results in an irradiance of 1000 W/m² [10]. As a result, AM1.5 solar radiation is considered a standard for actually evaluating the performance of solar cells, as it is considered the optimal conditions for sunlight to reach the Earth's surface when it falls vertically into the atmosphere [11].

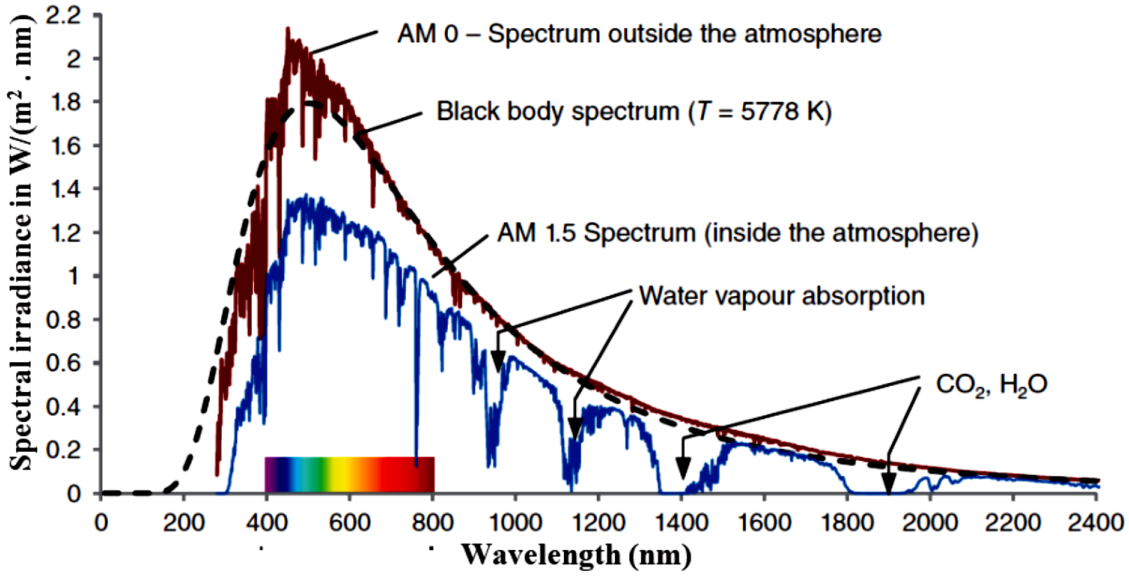

Figure 1.1: *Spectrum outside and inside the atmosphere.*

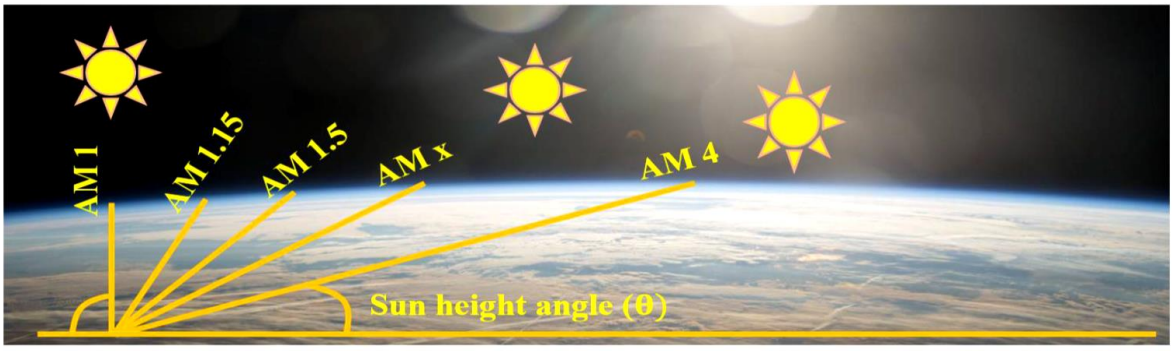

Figure 1.2: *Path of light in terms of Air Mass compared to the vertical distance to earth through the atmosphere.*

The impact of AM1.5 solar radiation on solar cells includes several key aspects:

1. Performance evaluation: By measuring and evaluating solar cell performance in a uniform and standardized manner, AM1.5 solar radiation makes it easier to compare various technologies and materials.
2. Design optimization: By understanding how a solar cell functions in AM1.5 conditions, one can enhance cell design and increase the cell's capacity to absorb solar energy.

3. Modifying production procedures: Manufacturing procedures can be modified to enhance the quality of solar cells by using performance data based on AM1.5 solar radiation [12].

1.3.Solar cells

1.3.1. The concept of solar cells

Solar cells are photovoltaic devices responsible for converting sunlight into electricity. Semiconducting materials such as silicone are used for this purpose. These materials generate electron- hole pairs when exposed to sunlight. The task of these couples is to generate power.

1.3.2. History of Solar Cells

There have been many scientific breakthroughs, innovations, and competitions in the history of solar cells. Although early solar cells were too inefficient to be of much use, solar energy has ancient roots and began to exist more than a century ago. Despite this, we frequently think of solar energy as a relatively modern technology [2]. In 1839, Edmond Becquerel discovered that two different brass plates immersed in a liquid produced a continuous electric current when exposed to sunlight. The PV effect in selenium was discovered in the late 1870s by Willoughby Smith, W. G. Adams, and R. E. Day [3]. The idea of generating power from the sun became a tangible prospect for the very first time. The scientific underpinnings of the photoelectric effect were little understood until Einstein published his 1905 paper explaining the photoelectric effect. It took over 100 years, from its discovery in 1839, for the first solar battery to become a reality In April 1954, researchers at Bell Laboratories demonstrated the first practical silicon solar cell [4]. In the early 2000s, research focused on new thin-film materials. Organic and organic-inorganic hybrids provide third- and fourth-generation solar cells, such as perovskites. These new materials allow solar cells to be printed on ultra-thin and flexible substrates [4].

1.3.3. Photovoltaic Effect

A.E. Becquerel, a French physicist, first described the "photovoltaic effect" in 1839. The term "photovoltaic effect" refers to the phenomenon wherein an object's charge distribution changes in response to illumination, resulting in the application of electromotive force and current. It first alludes to a process of energy conversion, namely the conversion of photons (light waves) into electrons and the conversion of photon energy into electron energy . It serves as the method for forming voltage, too. Gases, liquids, and solids can all have these effects; however, note that light energy is easily transformed into electricity in solids, especially semiconductors. As a result, interest in the photovoltaic effect in semiconductors has grown [16].

1.3.4. Working principle of solar cell

Two layers of semiconductors, one positive (p-type) and the other negative (n-type), make up conventional solar cells. The two described types are on the verge of creating a PN junction. A conductive current is created when incident photons with energy higher than the semiconductor's bandgap are absorbed by the material when the semiconductor is lit. This causes the electrons to move from the valence band into the conduction band. There is a positively charged hole for every negatively charged electron. The electric field sweeps holes and electrons in opposite directions close to the junction. Additionally, the electrons are driven to the external circuit by the electrode's motive force [5]. Light will be somewhat absorbed as it passes through a material once it has penetrated it. Electron-hole pairs are formed when photon energy surpasses the semiconductor's bandgap energy, as this is enough to break bonds and excite a valence electron into the conduction band, leaving a hole in the valence band. Photo generation is the term for this process, which is demonstrated in Figure 1.3.

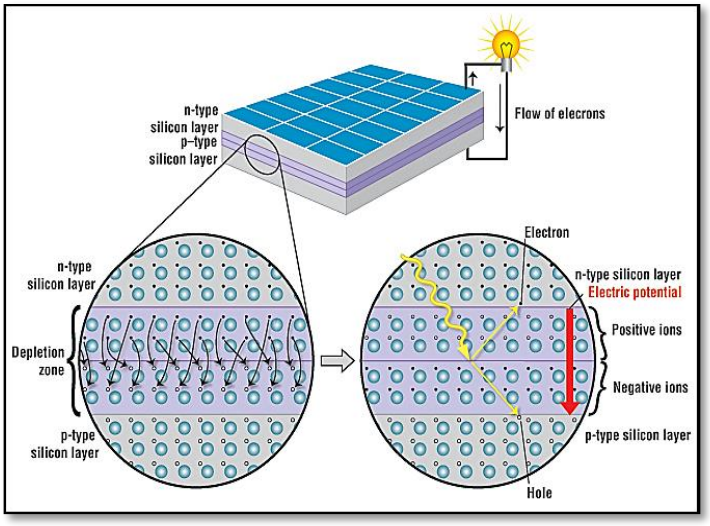

Figure 1.3: *An illustration that demonstrates the operation of a solar cell.*

1.3.5. P-N junction under illumination

In p-n junction semiconductor, more electron-hole pairs are generated when the p-n junction is illuminated. Minority carriers flow across the depletion region and into the quasi-neutral regions as a result of a significant increase in their concentration (holes in the n-type region and electrons in the p-type region). Electrons flow from the p-type region to the n-type region, while holes flow from the n-type region to the p-type region. The movement of these photo-generated carriers results in what is known as the photocurrent density, or J_{ph}, which increases the thermal generation current, or J_{gen}. When there is no external electrical connection between the n-type and p-type regions, the junction is in an open-circuit condition. Therefore, the reverse recombination current

must balance the current arising from the flow of thermally and photo-generated carriers. The electrostatic potential barrier across the depletion region will decrease, leading to an increase in the recombination current [7].

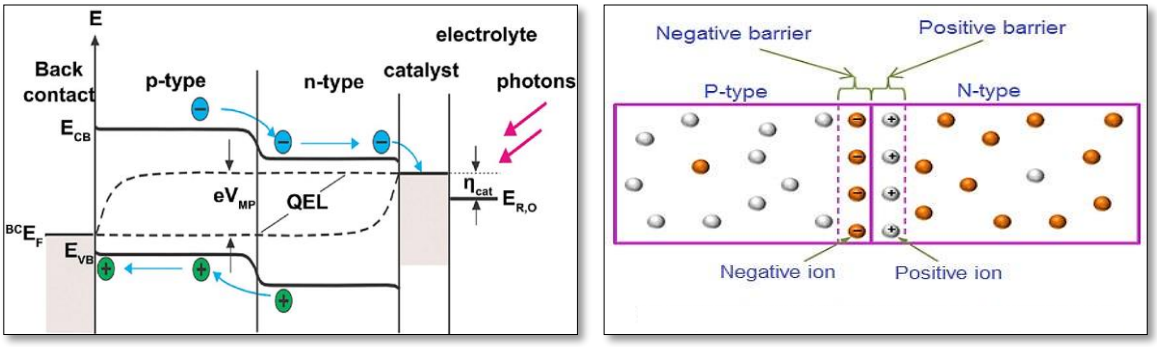

Figure 1.4: *P-N junction under illumination.*

1.3.6. Solar cell characteristics

The characteristics of a solar cell encompass open-circuit voltage, short-circuit current, fill factor, and photoelectric conversion efficiency.

1.3.6.1. Maximum power point (Pm)

The maximum power point (Pm) is determined in a solar cell when the power generation power is higher. This point is determined by monitoring the frequency current and the chemical generator effort and determining the point that disposes of the higher capacity. The determination of the maximum point depends on multiple concentration, such as temperature, density, and biometrics. DC-DC transformers are used to control efforts and agricultural currents for more extensive details. The term "Maxium Power Point Tracking (MPPT) " refers to precise details used to control the peak point in solar power cells. These details are considered to be capable of powering solar energy [8].

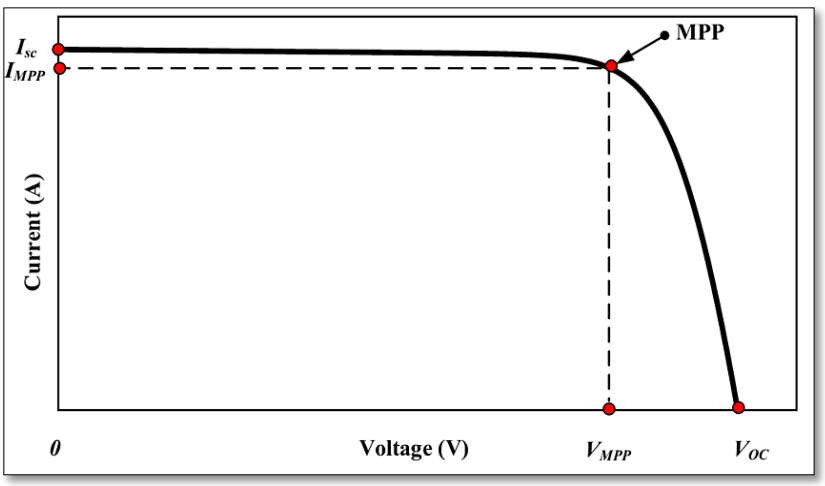

Figure 1.5*: curve for Maximum power point (Pm).*

1.3.6.2. Short circuit current (Isc)

The highest current that a solar cell or panel can produce when its terminals are short-circuited is known as short-circuit current (I_{sc}). It is a crucial factor in figuring out how well a solar cell works. Typically, standard test settings are used to measure the short-circuit current in order to give a consistent comparison between various solar cells [8]. When comparing solar cells of the same material type, the most critical material parameter is the diffusion length and surface passivation. In a cell with perfectly passivated surface and uniform generation, the equation for the short-circuit current density can be approximated as [9]:

$$J_{SC} = qG(L_n + L_p) \tag{1.1}$$

Where:

- G is the generation rate.
- L_n is the electron diffusion length.
- L_p is the hole diffusion length.

The short circuit current, I_{SC}, is the short circuit current density, J_{SC}, times the cell area:

$$I_{SC} = J_{SC} * A \tag{1.2}$$

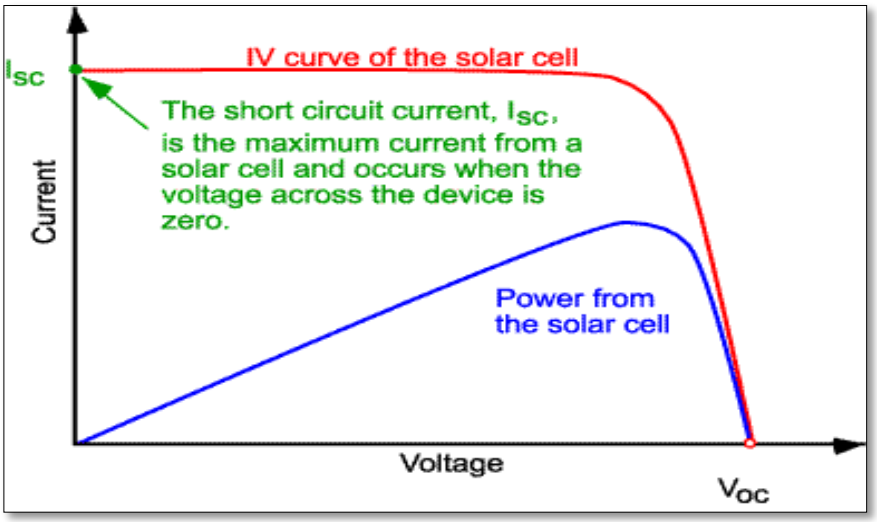

Figure 1.6: *curve for Short circuit current (I_{sc})*

1.3.6.3. Open circuit voltage (Voc)

Open circuit voltage (V_{oc}) is the maximum voltage that a solar cell, battery, or any other electrical device can produce when there is no load connected to it. It is a measure of the potential difference across the terminals of the device in an open circuit condition [9].

An equation for V_{oc} is found by setting the net current equal to zero in the solar cell equation to give:

$$V_{oc} = \frac{nkT}{q} ln\left(\frac{I_L}{I_0} + 1\right) \quad (1.3)$$

The V_{oc} can also be determined from the carrier concentration:

$$V_{oc} = \frac{kT}{q} ln\left[\frac{(N_A+\Delta n)\Delta n}{n_i^2}\right] \quad (1.4)$$

Where:

- Dark Saturation Current, I_0.
- Light Generated Current, I_L.
- Ideality Factor, n.
- Temperature, T.
- Doping Concentration, N_A.
- Excess Carrier Concentration, Δn.
- Intrinsic Carrier Concentration, n_i .

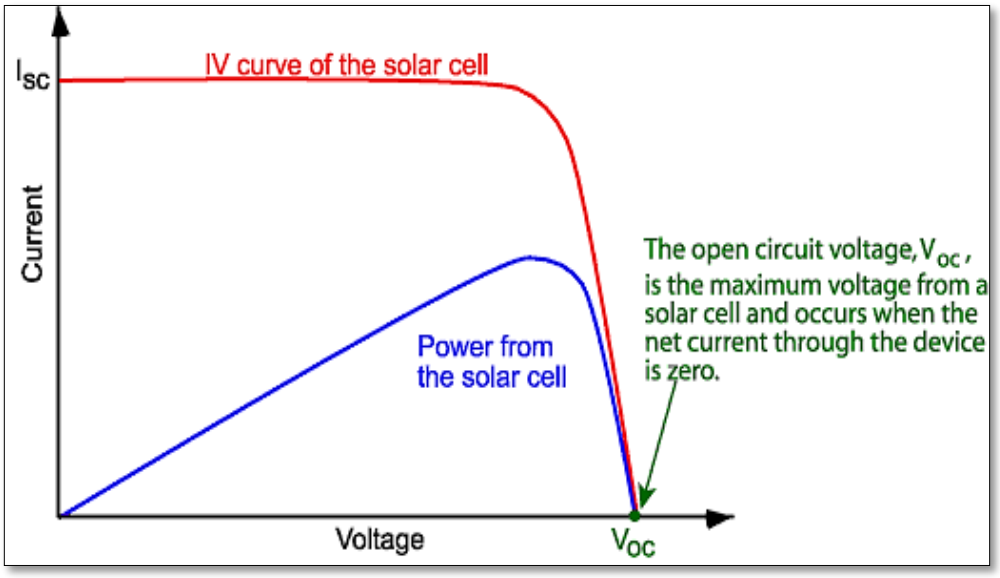

Figure 1.7: *curve for Open circuit voltage.*

1.3.6.4. Fill Factor (FF)

The fill factor (FF), which represents the ratio of the amount of electrical power that can be created to the total amount of power that can be extracted from an electrical device, is a metric used to evaluate the efficiency of solar cells and other electrical devices. It is computed by dividing the maximum amount of electricity that could be produced under perfect working conditions by

the ratio of the electrical power that is actually produced by the device and the amount that is extracted from it [9]. The equation of Fill Factor (FF):

$$FF = \frac{V_{MP}\, I_{MP}}{V_{OC}\, I_{SC}} \tag{1.5}$$

Where:

- Open-circuit voltage, V_{oc}.
- Short-circuit current, I_{sc}.
- Voltage at max power, V_{MP}.
- Current at max power, I_{MP}.

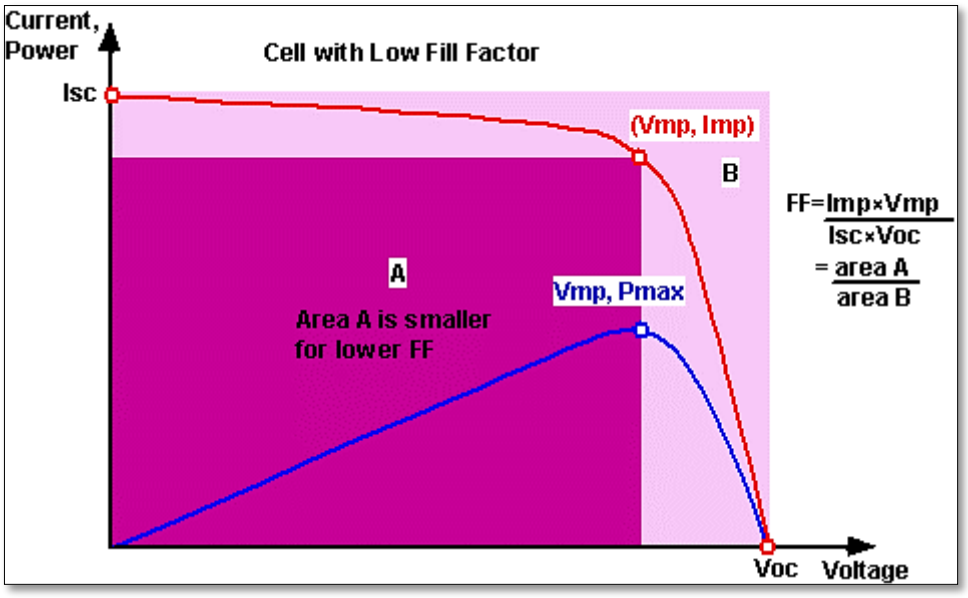

Figure 1.8: *curve for Fill Factor (FF).*

1.3.6.5. Efficiency

The most widely used metric for contrasting the performance of different solar cells is their efficiency. The ratio of the solar cell's energy output to its solar energy input is known as efficiency. The efficiency is dependent on the temperature of the solar cell as well as the spectrum and intensity of the incident sunlight. It also reflects the performance of the solar cell itself. Therefore, in order to evaluate the performance of different devices, the parameters under which efficiency is measured need to be properly controlled. Measurements of terrestrial solar cells are conducted at 25°C and AM1.5 conditions [9]. defined as:

$$\eta = \frac{V_{OC}\, I_{SC}\, FF}{P_{in}} \tag{1.6}$$

Where:

- V_{oc} is the open-circuit voltage.
- I_{sc} is the short-circuit current .
- FF is the fill factor .
- Input Power, P_{in} .

1.3.7. The equivalent circuit of a solar cells

The equivalent circuit of a solar cell consists of an ideal current generator in parallel with a diode in reverse bias, both of which are connected to a load. The generated current is directly proportional to light intensity. This highlights how important it is to accurately replicate the solar spectrum when testing solar cells, and why solar simulators are an indispensable piece of equipment in this context. Although the amount of current produced varies with light intensity, there are other limitations in solar cells which cap their efficiency. These limitations are represented by the other components in the circuit [4].

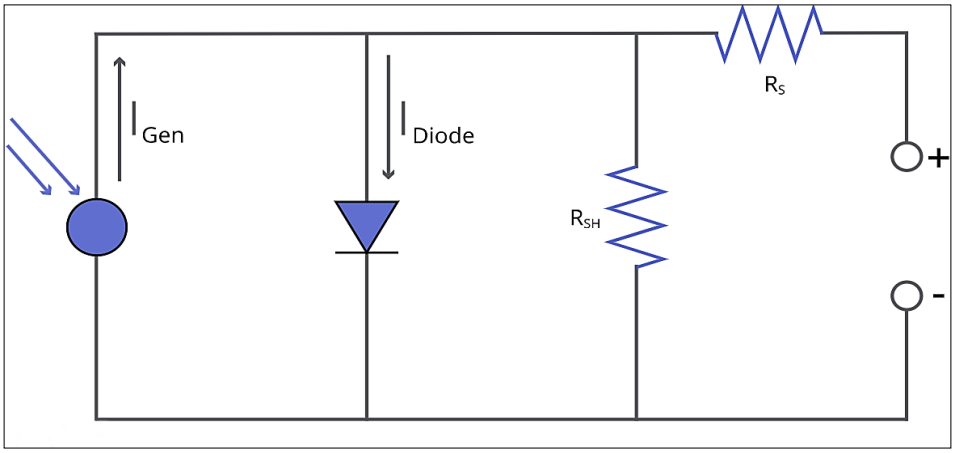

***Figure 1.9**: Equivalent circuit diagram of a solar cell.*

Parallel to this ideal current generator is a diode. The power that can be extracted from a device (P) is equal to current (I) multiplied by voltage (V):

$$P = V \times I \tag{1.7}$$

It is possible to derive equations that describe and simulate solar cells from this perfect circuit design. Additionally, this aids in the definition of several critical parameters that we employ to characterize solar cells. The amount of current created less the current passing through the diodes and the current lost due to shunt resistance is the easiest way to define current through the load.

$$I = I_{Gen} - I_{Diode} - I_{sh} \tag{1.8}$$

where I is current extracted, I_{Gen} is the generated current, I_{Diode} is diode current, and I_{sh} is current lost to shunt resistance. This equation gives us the characteristic current-voltage graph shape we see for solar cells.

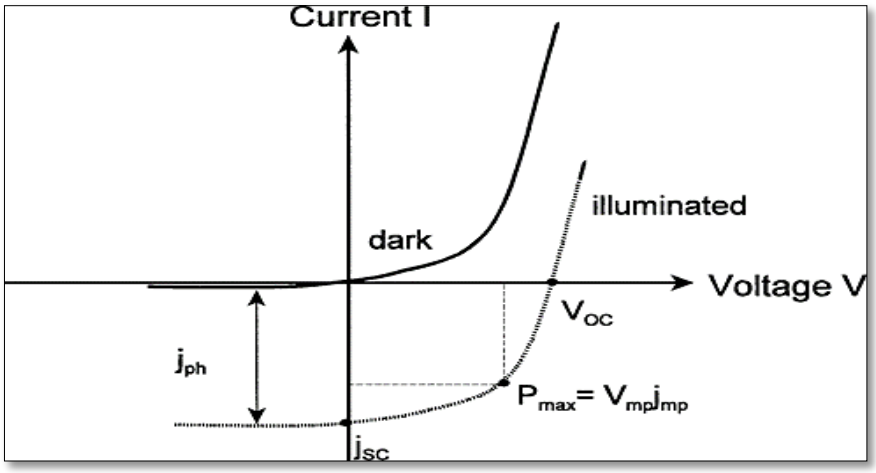

Figure 1.10: *The dark and illuminated I-V characteristics of the solar cell.*

1.3.8. Quantum efficiency

When a solar cell is exposed to light radiation, its ability to convert light into electricity is measured using a concept known as quantum efficiency. The number of electrons produced in a solar cell as a result of photons (light particles) being absorbed divided by the number of photons that enter the cell is known as quantum efficiency [8].

1.3.8.1. External Quantum Efficiency EQE

EQE, or External Quantum Efficiency, is the ratio of the number of charge carriers collected by the solar cell to the number of incident photons of a given energy shining on the solar cell. This measurement accounts for the reflection losses of the solar cell [7]:

$$EQE(\lambda) = \frac{Number\ of\ collected\ electron{-}hole\ pairs}{Number\ of\ incident\ photons} = \frac{Isc}{P_{in}} \cdot \frac{hc}{q\lambda} \qquad (1.9)$$

Where:

- P_{in} is incident power.
- Isc is Short circuit current
- h is Planck constant (6.626×10^{-34}).
- λ is wavelength of the incident photons
- c is speed of light (2.998×10^{8}).

1.3.8.2. Internal Quantum Efficiency IQE

Internal Quantum Efficiency (IQE) is the ratio of the number of charge carriers collected by the solar cell to the number of photons of a specific energy that are absorbed by the cell. Unlike External Quantum Efficiency (EQE), IQE does not take into account the losses due to reflections. The formula for IQE is given by [7]:

$$IQE = \frac{Number\ of\ collected\ electron{-}hole\ pairs}{Number\ of\ absorber\ photons} = \frac{EQE}{1-R} \tag{1.10}$$

where R is the reflection coefficient from the top surface of solar cell.

1.3.9. Loss mechanisms in Solar Cells

Cell losses are a major issue since they drastically lower cell efficiency; some losses can be prevented, but certain losses are inherent to the system. Since there are two main categories of losses, the majority of these losses are represented in the following figure: both electrical and optical.

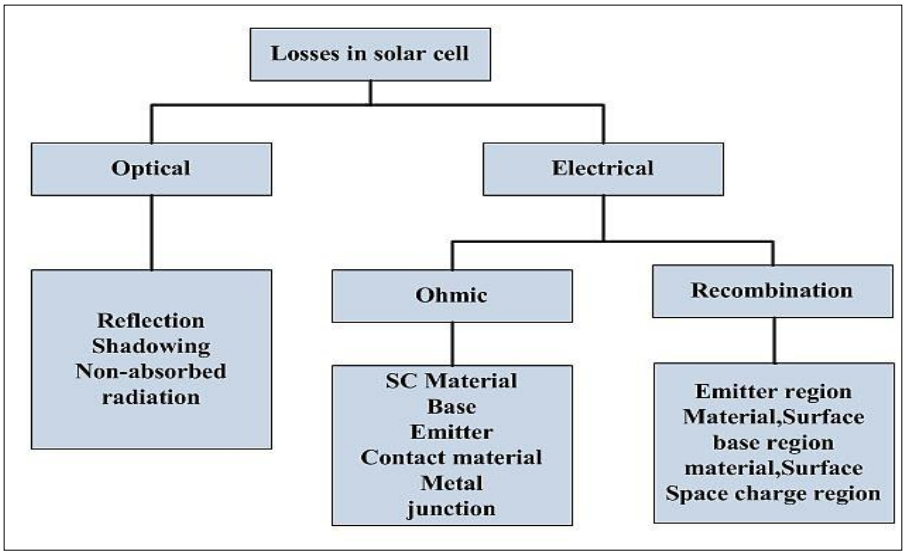

Figure 1.11: *Different losses in the solar cell.*

1.3.9.1. Optical losses in the solar cell

It is the reduction in solar energy absorption by the solar cell due to various optical variables. Surface reflection, internal reflection, and undesired absorption in passive materials are a few examples of these variables [14].

1.3.9.2. Electrical losses in the solar cell

Electrical losses in solar cells primarily arise from several factors. Narrow and elevated fingers on the cell's top surface help reduce electrical losses at the contact points. Despite this, the limited conductivity of the doped semiconductor results in ohmic losses, which diminish the cell's overall efficiency. Enhancing the n-doping level of the semiconductor can improve performance, but it also leads to increased recombination rates. Additionally, creating a junction between the semiconductor and metal, known as a Schottky contact, introduces a potential step that lowers the open circuit voltage of the solar cell [15].

1.3.10. Different Types of Solar Cells

Solar cells are presently categorized into four main generations based on the period of development and the types of materials used in their production. Figure 1.12 provides a summary of these different generations of solar cells.

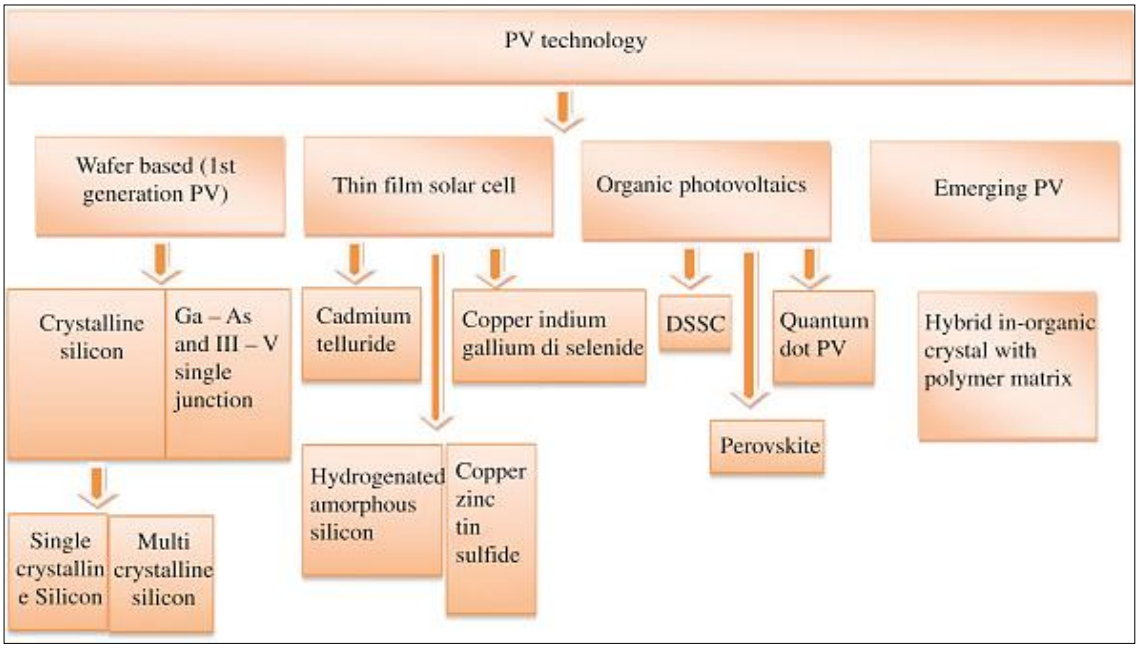

Figure 1.12: *Various generations of solar cells.*

NREL maintains a chart of the highest confirmed conversion efficiencies for research cells for a range of photovoltaic technologies, plotted from 1976 to the present [19]. Currently, the efficiency of perovskite solar cells has reached 26.7%, as depicted in Figure 1.13. This figure highlights the evolution of these cells over time and the progress made in other solar cell technologies.

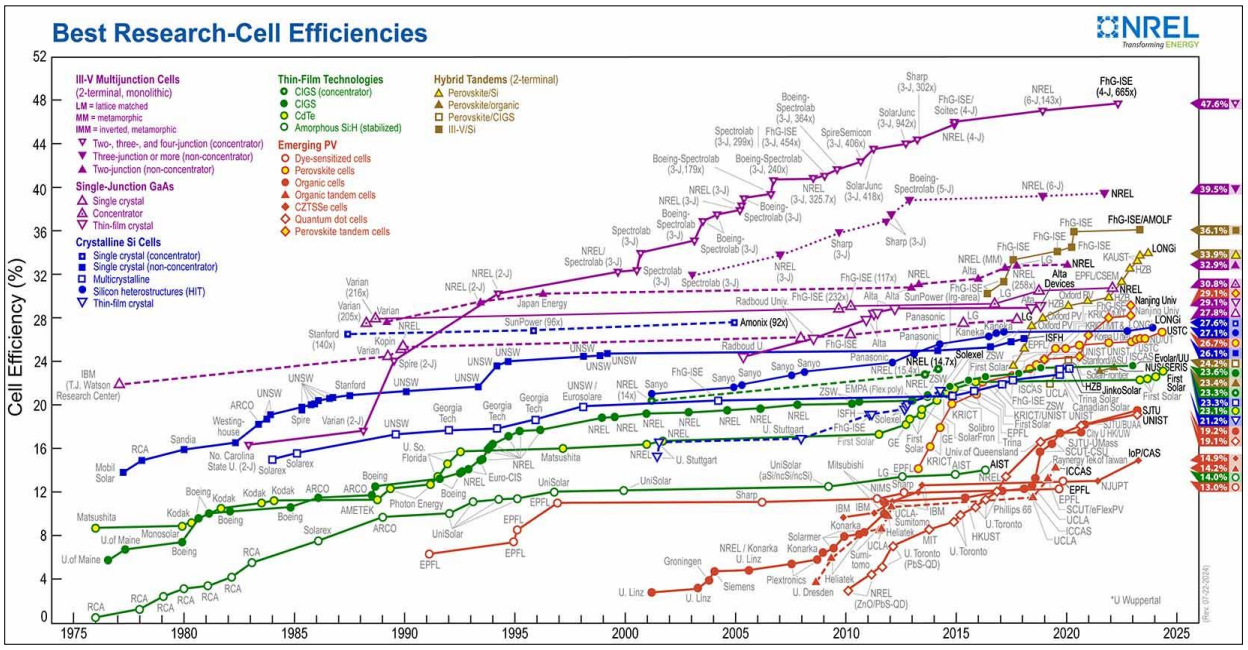

Figure 1.13: *Chart showing the highest research-cell efficiencies, adapted from [19].*

1.3.10.1. First generation: Silicon Solar Cells

The first generation consists of three types: Mono-crystalline, Multi-crystalline silicon, and Gallium Arsenide (GaAs) cells. These are among the oldest and most widely used cells due to their high efficiency, although they are expensive to manufacture. Since silicon is one of the most abundant materials in the Earth's crust, it suggests that the raw material will likely remain accessible in the future, potentially lowering its cost of acquisition [6].

a) Monocrystalline cells:

A monocrystalline silicon solar cell is one in which the silicon crystal forms as a single, uniform unit. Also referred to as monocrystalline solar cells (Mono-Si). Its regular crystalline structure, which minimizes obstructions to electron mobility, contributes to its great efficiency in converting solar energy into electrical power. Although the cost of production for these cells is often higher than that of polycrystalline cells, they offer superior performance and efficiency under various environmental circumstances [17]. The highest efficiency achieved in the laboratory for single-junction monocrystalline cells is 27.6% [14,19].

Figure 1.14: *The structure of Monocrystalline cells.*

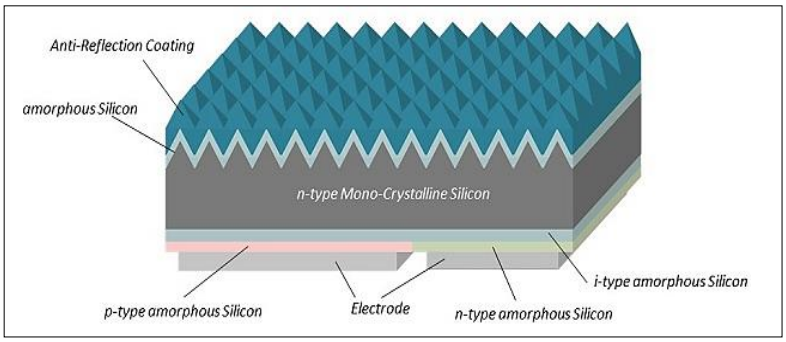

Figure 1.15: *A diagram showing the layers of a monocrystalline solar cell.*

b) Polycrystalline Solar Cells

This type of solar cell is made from silicon wafers containing numerous small crystals. Unlike monocrystalline cells, polycrystalline cells consist of multiple crystal grains, which simplifies the manufacturing process and reduces costs. However, their efficiency is generally slightly lower than that of monocrystalline cells because the boundaries between the crystals can impede the movement of electrons [18]. The highest efficiency achieved in the laboratory for single-junction polycrystalline cells is 23.3% [14,19].

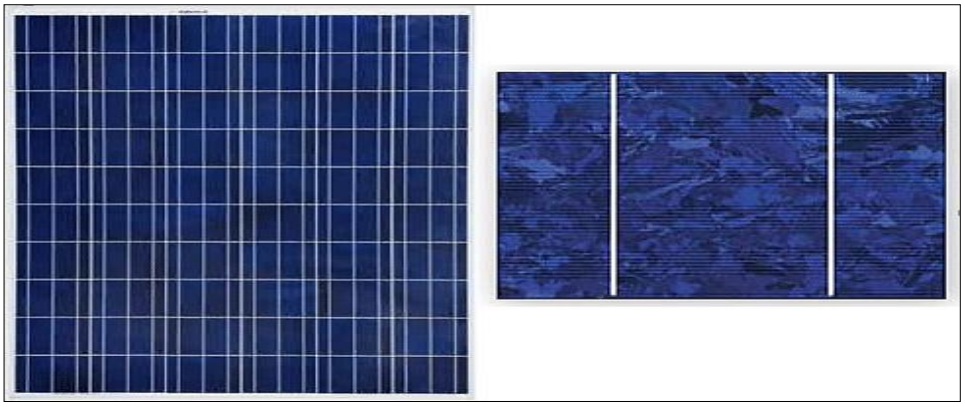

Figure 1.16: *The structure of Polycrystalline Solar Cells.*

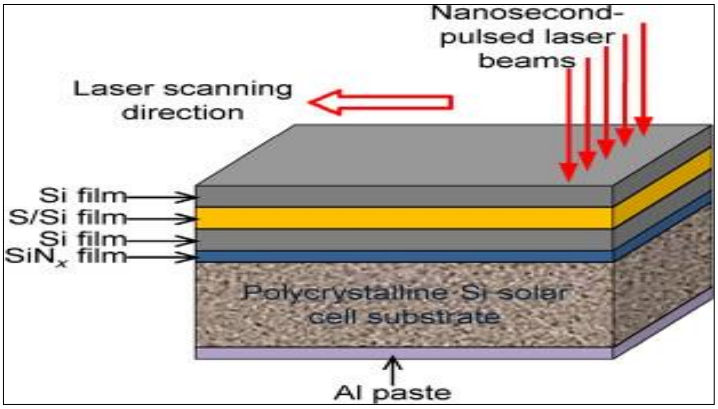

Figure 1.17: *A diagram showing the layers of a Polycrystalline Solar Cells.*

1.3.10.2. Thin film solar cells

Thin film solar cells, commonly referred to as second generation solar cells, are a kind of solar energy technology that converts light into electricity by using thin layers of semiconductor materials. Comparing these cells to conventional crystalline silicon solar cells reveals that they are lighter and thinner. These thin films are made from a variety of materials, including amorphous silicon (a-Si), copper indium gallium selenide (CIGS), and cadmium telluride (CdTe) [21]. In terms of performance, CdTe cells have achieved an efficiency of 23.1%, while CIGS cells have reached 23.6%. For a-Si cells, the efficiency is about 14% [14,19].

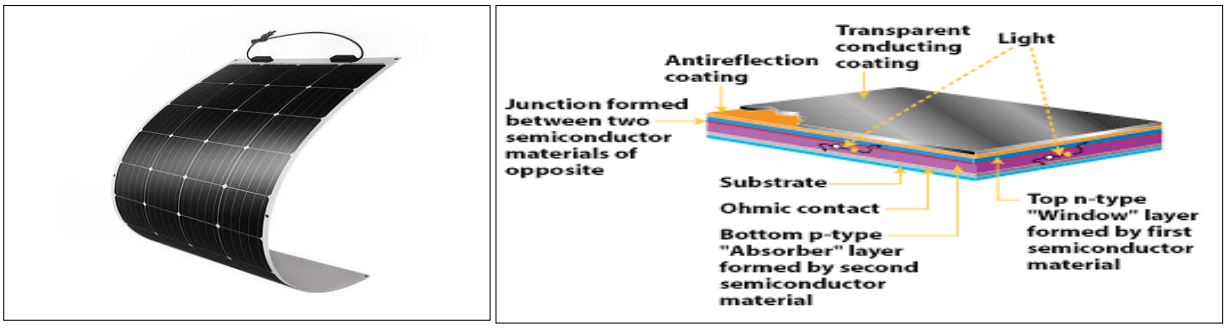

Figure 1.18: *The structure of Thin film solar cells and a diagram showing the layers of a Thin film solar cells.*

1.3.10.3. Third generation solar cells

Third-generation solar cells, similar to second-generation, are also made of thin films, but they are still in the emerging and developmental stages. Research is ongoing into the development of these third-generation thin-film solar cells using various organic and inorganic materials, such as perovskite solar cells. These cells are anticipated to achieve high power conversion efficiency (PCE) through the creation of multigap tandem cells, multiple exciton generation (MEG) capabilities, intermediate band (IB) formation, hot carrier conversion, and thermophotovoltaics. The exploration of new materials is also a key area of focus [23]. To date, perovskite solar cells have demonstrated an experimental efficiency of 26.7% [14,19].

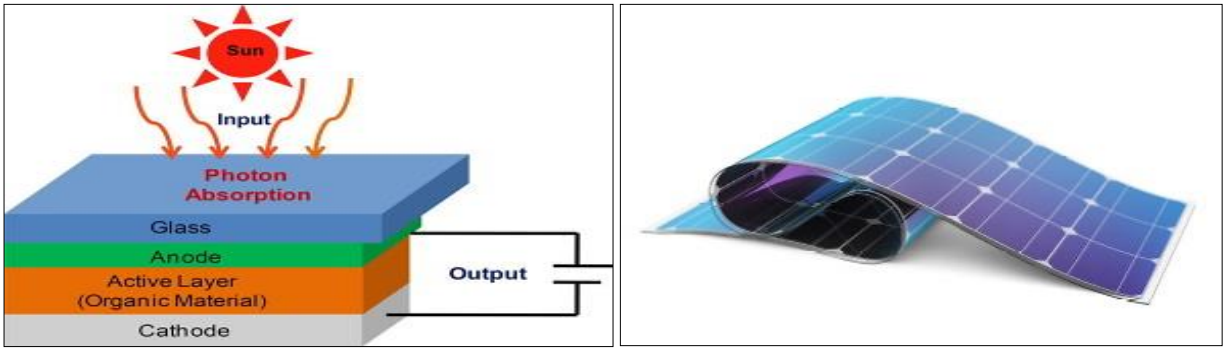

Figure 1.19: *The structure of organic solar cells and A diagram showing the layers of organic solar cells.*

References Chapter 1:

[1] Fahrenbruch, Alan, and Richard Bube. Fundamentals of solar cells: photovoltaic solar energy conversion. Elsevier, 2012.

[2] aps encourages the redistribution of the materials included in this newspaper providers.

[3] Fraas, Lewis M., and Larry D. Partain. Solar cells and their applications. John Wiley & Sons, 2010.

[4] https://www.ossila.com/pages/history-of-solar-cells

[5] Zhang, Chunfu, et al. Semiconductor photovoltaic cells. Springer, 2021.

[6] Luceño-Sánchez, J. A., Díez-Pascual, A. M., & Peña Capilla, R. (2019). Materials for photovoltaics: State of art and recent developments. *International journal of molecular sciences*, *20*(4), 976.

[7] Bajaj, N. S., & Joshi, R. A. (2021). Energy materials: synthesis and characterization techniques. In Energy materials (pp. 61-82). Elsevier.

[8] S.M. Sze, M.-K. Lee, Semiconductor Devices: Physics and Technology: Physics and Technology, Wiley Global Education, 2012.

[9] https://www.pveducation.org/pvcdrom/solar-cell-operation

[10] Brabec, Christoph J., N. Serdar Sariciftci, and Jan C. Hummelen. "Plastic solar cells." Advanced functional materials 11.1 (2001): 15-26.

[11] Marzo, Aitor, et al. "Comparison of Atacama desert solar spectra vs. ASTM G173–03 reference spectra for solar energy application." Conference Proceedings EuroSun. 2016.

[12] Green, M. A. (1998). "Solar Cells: Operating Principles, Technology, and System Applications". Prentice-Hall PTR. [13] Duffie, J. A., & Beckman, W. A. (2013). "Solar Engineering of Thermal Processes". John Wiley & Sons, Inc.

[14] Green, M. A., Dunlop, E. D., Yoshita, M., Kopidakis, N., Bothe, K., Siefer, G., ... & Hao, X. (2024). Solar cell efficiency tables (Version 64). *Progress in Photovoltaics: Research and Applications*.

[15] Shockley, W., & Queisser, H. J. (1961). "Detailed balance limit of efficiency of p-n junction solar cells". Journal of Applied Physics, 32(3), 510-519

[16] Green, Martin A. "Silicon photovoltaic modules: a brief history of the first 50 years." Progress in Photovoltaics: Research and applications 13.5 (2005): 447-455.

[17] Fraas , Lewis M., and Mark J. O'Neill. Low-cost solar electric power. New York: Springer, 2014.

[18] Green, Martin A. "Solar cells: operating principles, technology, and system applications." Englewood Cliffs (1982).

[19] Best research-cell efficiencies chart. NREL, (n.d.). https://www.nrel.gov/pv/cell-efficiency.html (accessed august 08, 2024).

[21] Chopra, K. L., P. D. Paulson, and Viresh Dutta. "Thin-film solar cells: an overview." Progress in Photovoltaics: Research and applications 12.2-3 (2004): 69-92.

[22] MERTENS, Konrad. Photovoltaics: fundamentals, technology, and practice. John Wiley & Sons, 2018.

[23] Mondal, S., Manna, A. S., & Maiti, D. K. (2021). Nanotools and devices in solar power energy. In Nano Tools and Devices for Enhanced Renewable Energy (pp. 429-446). Elsevier.

Chapter 2: Perovskite Solar Cell and SCAPS simulation program

2.1. Introduction

The perovskite layer is a crucial component in composite solar cells, playing a vital role in converting light into electrical current. Perovskite materials possess unique properties that make them ideal for highly efficient light absorption and effective electrical charge transmission. Typically composed of metal-organic compounds with a three-dimensional crystal structure, such as $CsPbIBr_2$, these materials exhibit high light absorption across the solar spectrum, enabling them to generate electrical current with high efficiency. Additionally, the perovskite layer's superior electrical conduction properties facilitate the movement of electrons and electron holes within the solar cell. The study and development of perovskite layers is an active field in renewable energy, with their integration in composite solar cells representing a significant step toward achieving higher efficiency in light-to-electricity conversion [1].

In this chapter, we will define perovskite materials, particularly those used in our simulations, such as $CsPbIBr_2$ and $KSnI_3$. We will also introduce the simulation software SCAPS-1D, detailing its operation and the steps required for successful solar cell simulation. This will provide the reader with a clear understanding of the software and its application in our research.

2.2. Perovskite cell

The term "perovskite" does not designate any specific material, like silicon or cadmium telluride. Instead, it encompasses a whole family of compounds. These substances are referred to as "perovskite," named after the mineral discovered in 1839, which was named after Russian mineralogist L.A. Perovski. The original mineral perovskite (calcium titanium oxide, or $CaTiO_2$) consists of three distinct components: A, B, and X. Its crystal structure is distinct [2].

The perovskite layer is appealing for use in solar cells because of several benefits, such as:

1. **High light absorption efficiency:** One of the unique qualities of the perovskite layer is its high light absorption efficiency, which helps convert the most light into electrical current.
2. **Manufacturing simplicity:** The perovskite layer is easier to make and install than other solar cell materials, which reduces production costs.
3. **High conversion efficiency:** Studies show that the perovskite layer converts light into electrical current with high efficiency.

Typically, the perovskite layer is utilized in conjunction with other layers to enhance cell stability and conversion efficiency in multilayer solar cell structures. Perovskite technology represents one

of the most significant recent advancements in the field of solar energy, marking a critical step in raising solar cell efficiency [2].

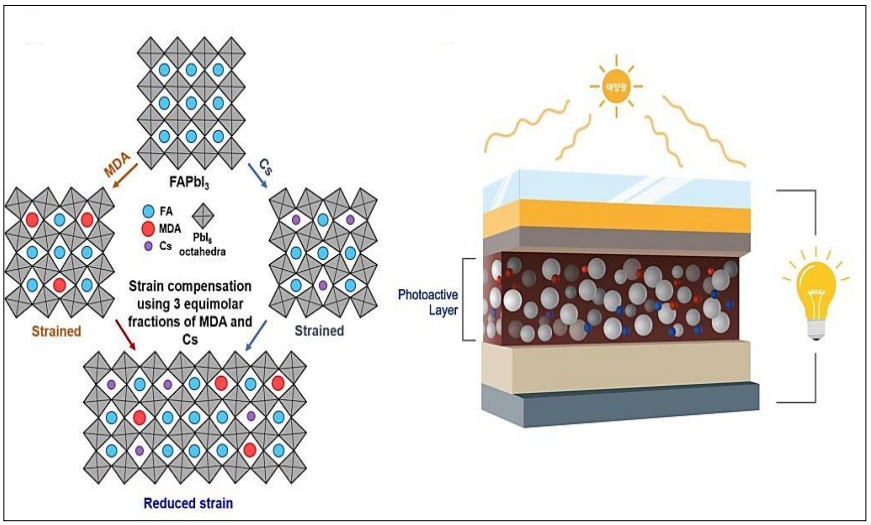

***Figure 2.1**: Shows the general cubic crystal structure of perovskites.*

2.2.1. Composition and Components of the Perovskite Layer in Solar Cells

As we said before, in perovskite solar cells, the perovskite layer is composed of a mixture of organic and inorganic materials. The general formula for the perovskite structure is ABX_3 [11], where:

- **A** is an organic or inorganic monovalent cation, typically methylammonium ($CH_3NH_3^+$), formamidinium ($CH(NH_2)_2^+$), cesium (Cs^+), or potassium (K^+) etc.
- **B** is an inorganic cation, usually a metal like lead (Pb^{2+}) or tin (Sn^{2+}), etc.
- **X** is a halide anion, such as chloride (Cl^-), bromide (Br^-), or iodide (I^-), etc.

a) Organic Materials:

- ✓ **Methylammonium ($CH_3NH_3^+$):** A common organic cation used in many perovskite formulations.
- ✓ **Formamidinium ($CH(NH_2)_2^+$):** Another organic cation that can be used to improve stability and efficiency.
- ✓ **Polymeric Hole Transport Materials (HTMs):** Organic materials such as Spiro-OMeTAD, PEDOT, etc., are often used to transport holes in the perovskite structure.

b) Inorganic Materials:

- ✓ **Lead (Pb^{2+}):** The most common metal cation used in perovskite solar cells, forming compounds like methylammonium lead iodide ($CH_3NH_3PbI_3$).

- ✓ **Tin (Sn^{2+}):** Used as an alternative to lead, though it is less stable.
- ✓ **Cesium (Cs^{+}):** An inorganic cation used to enhance the stability of the perovskite structure.
- ✓ **Halide Anions (Cl^{-}, Br^{-}, I^{-}):** These halides form the X component of the ABX_3 structure and are crucial in determining the optical and electrical properties of the perovskite [1,11].

These materials work together to form a highly efficient and flexible light-absorbing layer in perovskite solar cells.

2.2.1.1. Potassium Tin iodide ($KSnI_3$)

The perovskite research community is currently interested in the compound $KSnI_3$ as a potential replacement for other toxic and relatively expensive materials such as $MAPbI_3$, $CsPbI_3$, and $RbPbI_3$ used in photovoltaic devices [11]. $KSnI_3$ stands out due to its non-toxic nature and features a band gap of 1.84 eV, coupled with a high absorption coefficient. These attributes make $KSnI_3$ a strong candidate for application in solar cells [13,14]. $KSnI_3$ is created by combining potassium (K^{+}), tin (Sn^{2+}), and iodide (I^{-}), as shown in Figure 2.2, which illustrates the orthorhombic structure of $KSnI_3$.

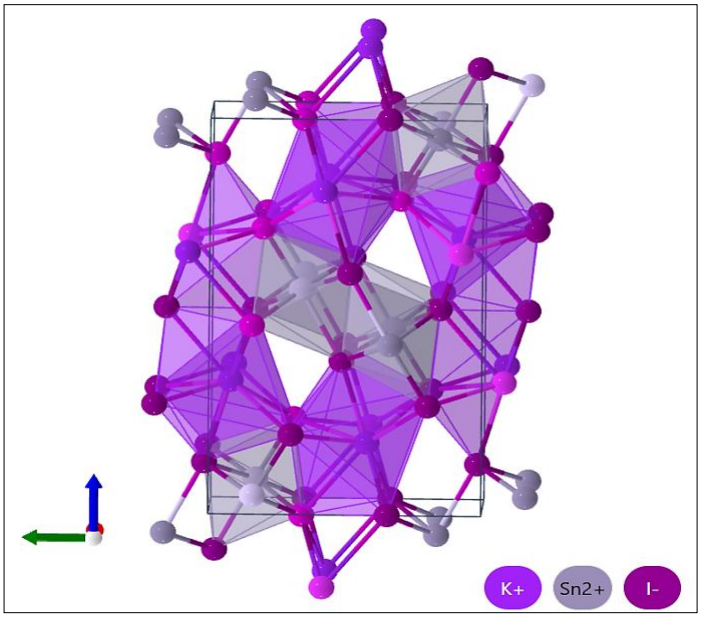

Figure 2.2: *Orthorhombic structure of $KSnI_3$ [12].*

As an emerging material, $KSnI_3$ has not yet been extensively studied, and there are no prior experimental reports on perovskite solar cells based on $KSnI_3$ in the existing literature. In contrast, Pindolia et al. conducted a DFT study of $KSnI_3$ and, using the SCAPS simulator, proposed a new single-junction $KSnI_3$ solar cell that achieved a PCE of 9.776% [13]. Whereas Kundara et al., also

using the SCAPS simulator and a machine learning model, proposed the FTO /WS_2/$KSnI_3$/PEDOT/Au configuration, which achieved a higher PCE of 23.08% [14]. To date, only a limited number of theoretical studies have reported on $KSnI_3$-based PSCs.

2.2.1.2. Cesium lead iodide bromide ($CsPbIBr_2$)

Cesium lead iodide bromide ($CsPbIBr_2$) is a halide perovskite material composed of cesium (Cs), lead (Pb), iodine (I), and bromine (Br), as shown in Figure 2.3. The general structure of $CsPbIBr_2$ is described as a mixed-halide perovskite, a material that has gained significant attention in the field of photovoltaics, particularly in the development of PSCs. Recent research efforts have increasingly focused on mixed halide perovskites like $CsPbI_2Br$ and $CsPbIBr_2$. While $CsPbI_2Br$ features a narrow band gap of 1.92 eV, it is susceptible to degradation under extreme heat or high humidity, which compromises its reliability. On the other hand, $CsPbIBr_2$ not only possesses a suitable band gap of 2.08 eV but also demonstrates remarkable high-temperature stability exceeding 460°C and a low phase transition temperature around 100°C. These attributes make $CsPbIBr_2$ an ideal perovskite material, known for both high efficiency and stability. Nevertheless, challenges persist with $CsPbIBr_2$ PSCs, resulting in a power conversion efficiency (PCE) that remains considerably below its theoretical limit, as defined by the Shockley-Queisser limit of 20.5% [3].

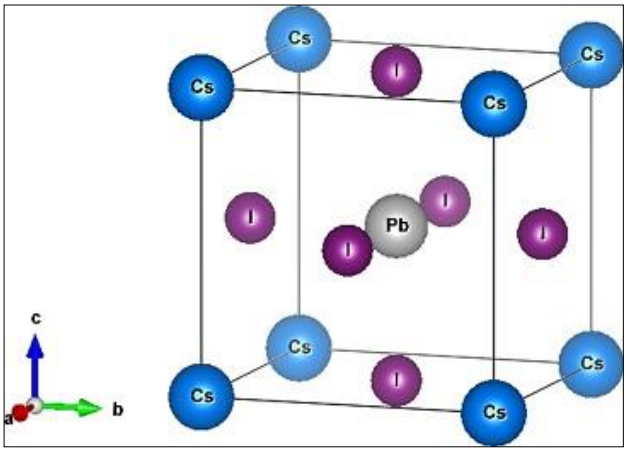

Figure 2.3: *The crystal structure of unit cell of $CsPbIBr_2$.*

Recently, several studies have focused on $CsPbIBr_2$ PSCs. Experimentally, using a $CsPbIBr_2$ single junction, Khan et al. achieved a PCE of 9.71% with an FTO/TiO_2/$CsPbIBr_2$/Spiro/Au structure [9]. Additionally, Sheng et al. achieved an efficiency of 9.6% using $CsPbIBr_2$ as the absorber layer and SnO_2 as an electron transport layer (ETL) [16]. Theoretically, Khatoon et al. utilized $CsPbI_2Br$ and $CsPbIBr_2$ as two absorber layers to form a $CsPbIBr_2$/$CsPbI_2Br$ bilayer PSC, achieving an efficiency of 20.62% [17].

2.2.1.3. Tin Oxide (SnO_2)

In nature, tin oxide (SnO_2), also known as stannic oxide, is found as the mineral cassiterite. With a tetragonal unit cell and the rutile crystal structure, it has the lattice constants a = b 4.738 Å, c = 3.188 Å, and u = about 0.307, which stands for the separation of the Sn and O atoms. Figure 2.4 schematically depicts the crystal structure of SnO_2, making it evident that each Sn atom has six nearest oxygen neighbors, forming a deformed octahedron. The oxygen octahedron's core is occupied by Sn atoms. An estimate of the SnO_2 band gap is 3.6 eV. To enhance the electrical and optical characteristics of n-type SnO_2, a variety of dopants are used, including fluorine (F), antimony (Sb), arsenic (As), phosphorus (P), molybdenum (Mo), etc. Conversely, for the p-type SnO_2, doping like aluminum (Al), gallium (Ga), zinc (Zn), etc. is used [5]. We extract FTO (fluorine-doped tin oxide), a transparent semiconductor material with an energy gap of 3.2 to 3.6 electron volts (ev), from the SnO_2 doping process. FTO is used as a light-guiding layer in solar cells and works to increase the efficiency of converting light into electrical energy [6]. Additionally, SnO_2 is utilized as an ETL in solar cells.

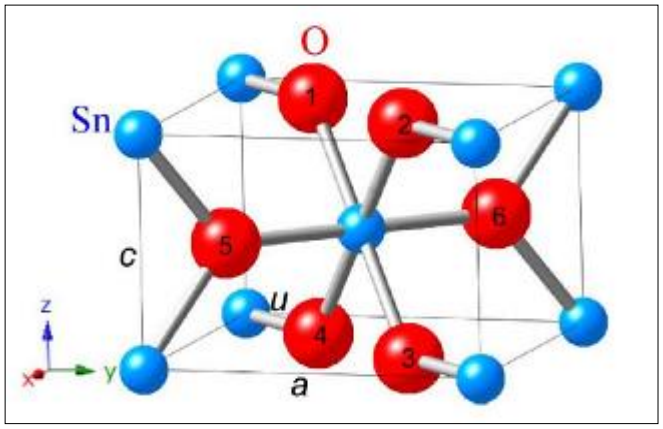

Figure 2.4: *The crystal structure of unit cell of SnO_2.*

2.2.1.4. Spiro-OMeTAD

Spiro-OMeTAD is a common hole transport material (HTL) used in perovskite solar cells and other types of photovoltaic devices. It facilitates the transport of positive charge carriers (holes) from the light-absorbing layer to the electrode, thereby improving the efficiency of the solar cell. Its full chemical name is 2,2',7,7'-Tetrakis[N,N-di(4-methoxyphenyl)amino]-9,9'-spirobifluorene .This material has high hole mobility and good stability, which makes them suitable for use in perovskite solar cells [18]. It has a wide band gap of 2.85 eV [19]. Spiro-OMeTAD as an organic small molecule TTM is most widely employed to fabricate perovskite devices capable of high PCE more than 20%. As a rare merit among other organic materials it can work as a thickness HTL >200 nm, which facilitates coating of HTL even on rough surfaces of perovskite grains [20].

2.3.The simulation

Solar cell simulation software is computer tools used to model and analyze the performance of solar cells virtually. These programs aim to simulate the behavior of a solar cell under various conditions and variables, such as lighting intensity, temperature, and the properties of the materials used in manufacturing the cell. Solar cell simulation software models the process of converting solar light into electrical energy within the cell, using a variety of physical and mathematical models. These models include charge balance equations, transport equations, and compatibility equations, which allow the efficiency and electrical performance of a cell to be estimated under different conditions. Simulation software is a valuable tool for understanding the basics of how solar cells work and improving their design. They also provide the ability to test a new design idea or a change in cell parameters without having to actually manufacture it, saving time and costs. Popular programs used for solar cell simulation include SCAPS, Silvaco, PC1D, Centaurus TCAD, and others. These programs come with intuitive and versatile user interfaces, making it easy for researchers and engineers to use them to study and analyze solar cells accurately and effectively.

2.3.1. SCAPS-1D

The Electronics and Information Systems (ELIS) department at the University of Ghent, led by M. Burgelman, developed a one-dimensional solar cell device simulator known as SCAPS-1D (Solar Cell Capacitance Simulator) [21]. The PV research community can freely access SCAPS. A solar cell can be conceptualized as a stack of up to seven layers, each having distinct characteristics including thickness, doping, optical absorption, defect densities, and defect dispersion. The following common measures can then be simulated: I-V, QE, C-V, and C-f. SCAPS-1D is highly popular among solar cell simulators because its simulated results show excellent agreement with experimental data [3]. In the present study, SCAPS-1D version 3.3.07 was utilized due to its advantages, including ease of use and control, the ability to simulate both illuminated and dark conditions, and the capability to design a heterostructure system with up to seven layers [22].

2.3.1.1. Simulation equations

To achieve the desired results, the SCAPS software uses a one-dimensional diffusion system to solve Poisson's and continuity equations, taking into account the boundary conditions. This method allows for an accurate representation of the internal electric field and carrier behavior within the cell [7]. The most important of these equations that the program follows are:

a. Poisson's Equation: Equation (2.1) defines Poisson's equation, which describes the relationship between electrostatic potential and charge density [7,8,22].

$$\frac{\partial^2}{\partial^2 x}\varphi(x) = \frac{q}{\varepsilon_r}[p(x) - n(x) + N_D^+(x) - N_A^-(x) \pm N_t(x)\,] \qquad (2.1)$$

Here, the electrostatic potential is denoted by φ, the charge by q, and the static relative permittivity of the medium by ε_r. The electron and hole concentrations are represented by n and p, respectively, while the donor and acceptor densities are indicated by N_D^+ and N_A^-. Additionally, the defect densities of the acceptor and donor are represented by N_t.

b. Continuity equations: The continuity equation conveys a core concept: the change in carrier density over time is determined by the difference between the incoming and outgoing carrier flux, along with the effects of generation and recombination. The electron and hole continuity equations are formulated as follows [7,8,22]:

Continuity equation for the electron: $$\frac{\partial n}{\partial t} = \frac{1}{q}\frac{\partial J_n}{\partial x} + G_n - R_n \qquad (2.2)$$

Continuity equation for the hole: $$\frac{\partial p}{\partial t} = \frac{1}{q}\frac{\partial J_p}{\partial x} + G_p - R_p \qquad (2.3)$$

Where J_n and J_p represent the current densities of electrons and holes, G_n and G_p denote the carrier generation rates for electrons and holes, and R_n and R_p represent the recombination rates of electrons and holes, respectively.

c. Transport equation: Similarly, the carrier current density can be determined using the following transport equations for drift-diffusion (total current density) [7,8,23]:

$$J_n = nq\mu_n E + qD_n\frac{\partial n}{\partial x} \qquad (2.4)$$

$$J_p = pq\mu_p E + qD_p\frac{\partial p}{\partial x} \qquad (2.5)$$

Here, μ_n and μ_p refer to the mobilities of electrons and holes, respectively, while D_n and D_p denote the diffusion coefficients for electrons and holes, respectively. $\frac{\partial n}{\partial x}$ and $\frac{\partial p}{\partial x}$ represent the concentration gradients of electrons and holes, respectively.

2.3.1.2. Essential Steps for Conducting a Successful SCAPS Simulation

The key steps to ensure a successful simulation in SCAPS are as follows:

a. After we install the program on the computer, we click on the program icon to open it, and the main interface appears, as shown in Figure 2.5.

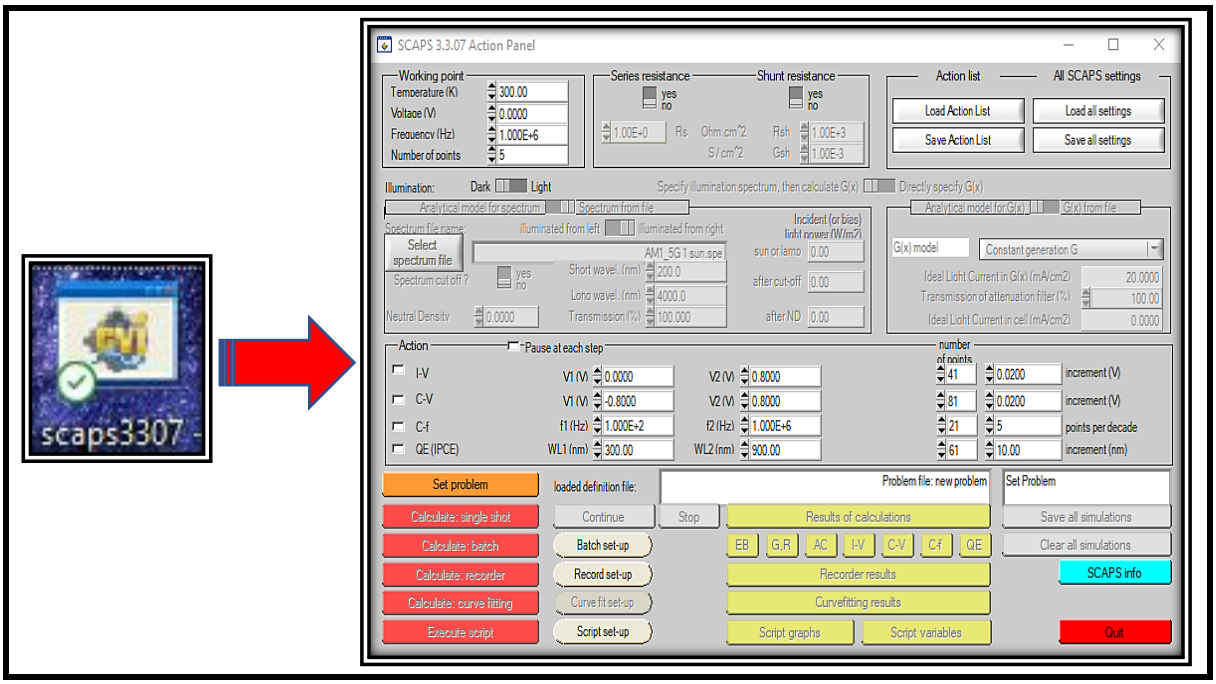

Figure 2.5: *The program icon and its main interface.*

b. We then change the scene from dark to light (1). Next, we specify the criteria we are examining and their scope (2,3). We click "Set Problems" to enter the materials and their attributes (4), as shown in Figure 2.6.

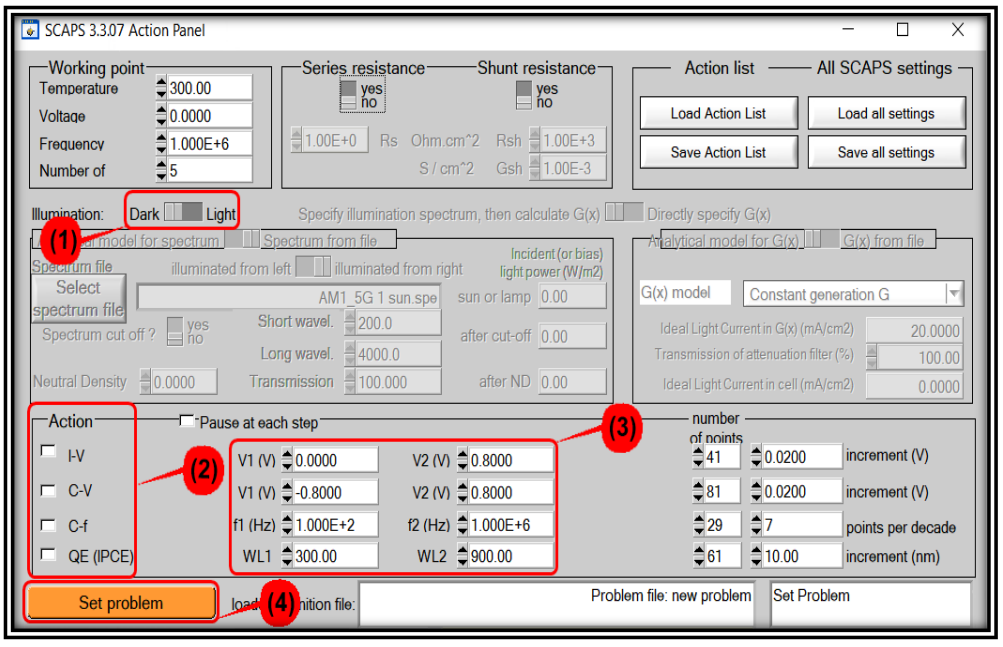

Figure 2.6: *The first steps to start the simulation.*

c. Clicking the 'Set Problems' button will cause the software to open a new interface. We can expand the layers section of this interface by adding new cell elements, as illustrated in Figure 2.7. The direction of the sun's beams is shown by arrows on the white box that holds the cell.

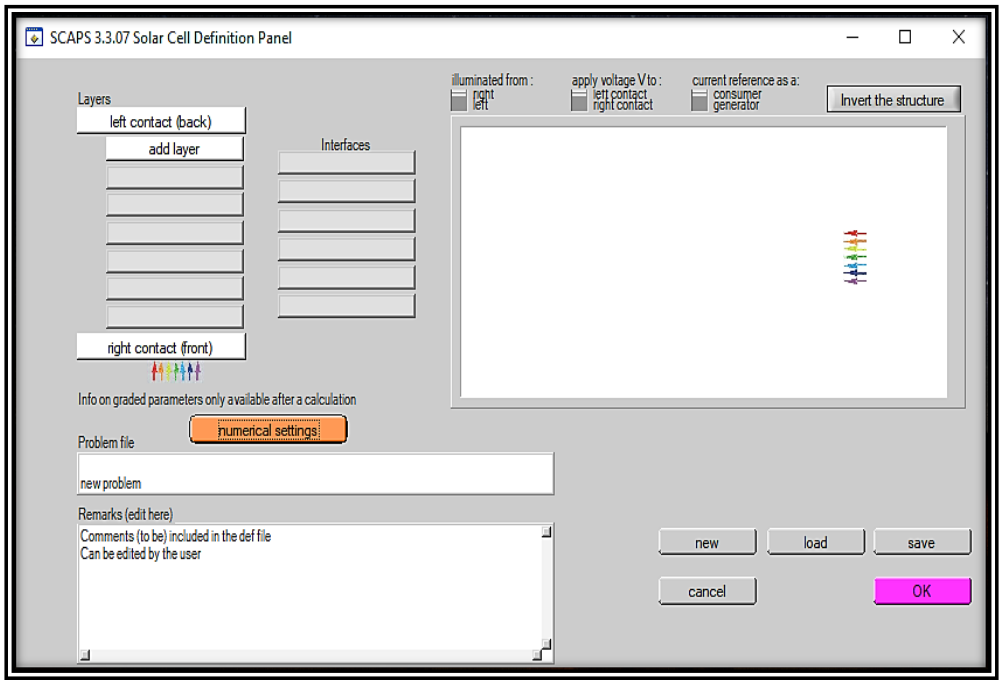

Figure 2.7: *A new interface for entering cell elements.*

d. As shown in Figure 2.7, there is a layered area. Click on the "Add Layer" button, which will open a new interface (see figure 2.8) where you can enter the material and its properties, including thickness, band gap, electron affinity, etc. Then press the "Add" button at the bottom to successfully add the material. Complete the rest of the materials using the same steps. If the material and properties are already registered or in the program database, you can load them by clicking the "Load Materials" button. For optical properties, we can add them by using the "Set Absorption Model" button or by importing from a file. To add defects, we use the "Add Defect 1" button.

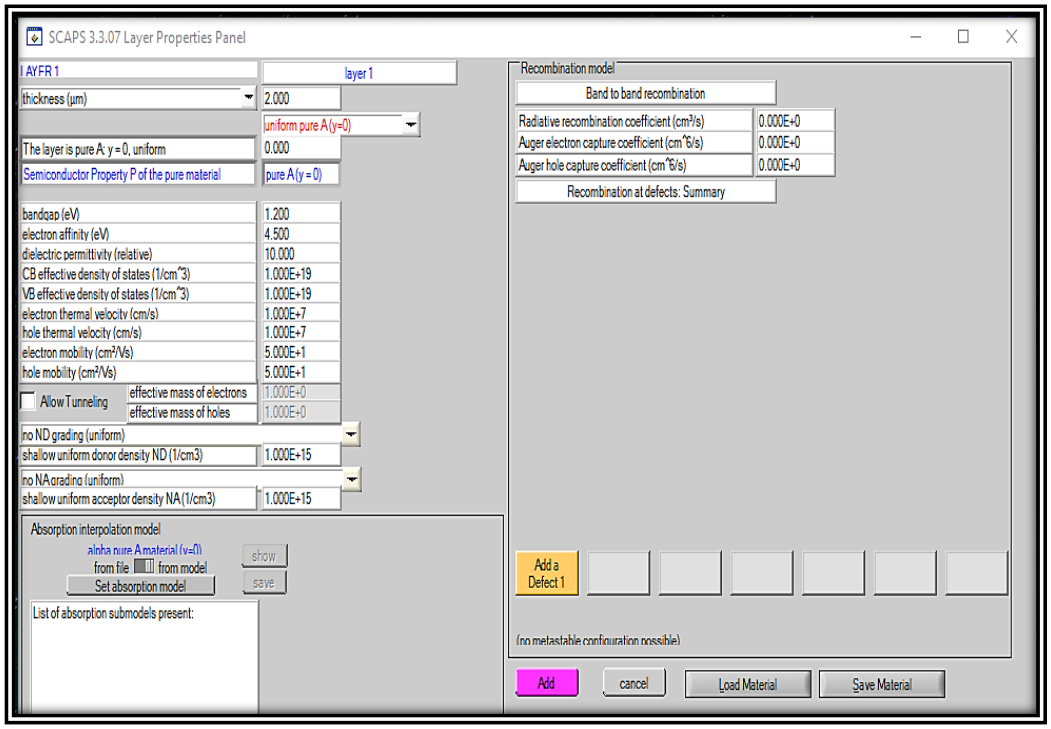

Figure 2.8: *Add cell layers and their properties.*

e. The front and back contact properties, such as Thermionic emission/velocity surface recombination and Metal work function, are adjusted by clicking either the front or back contact button on the cell definition panel (see Figure 2.9). This action opens the 'Contact Properties Panel', as shown in Figure 2.10.

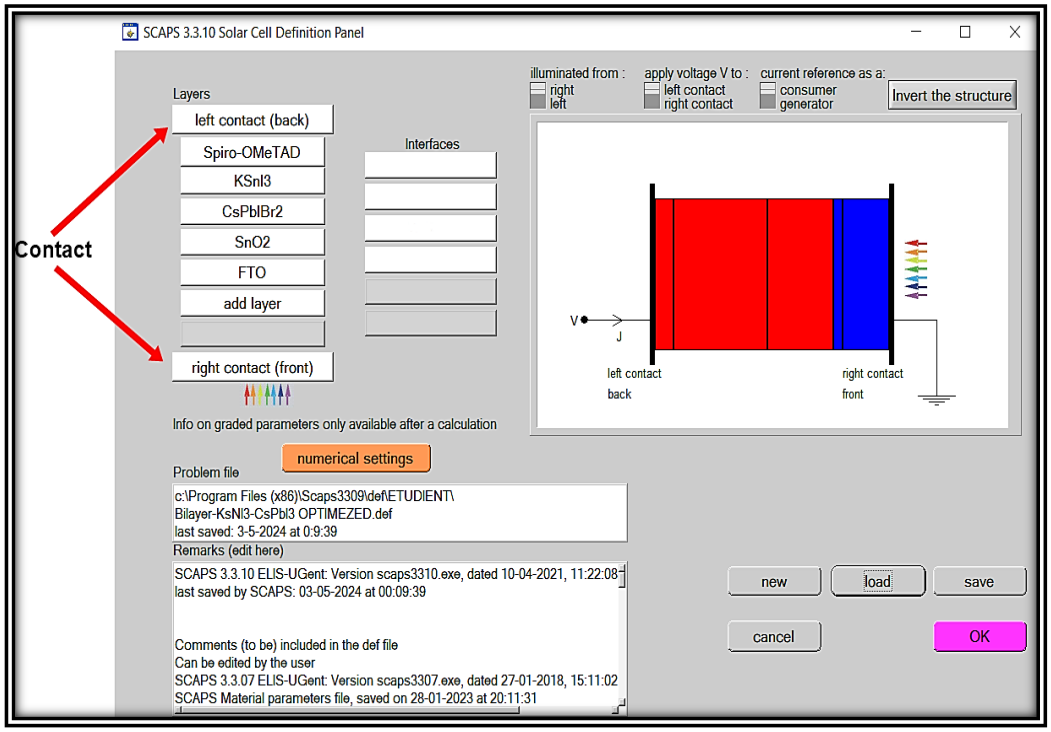

Figure 2.9: *Varying the Left and Back Contact Properties.*

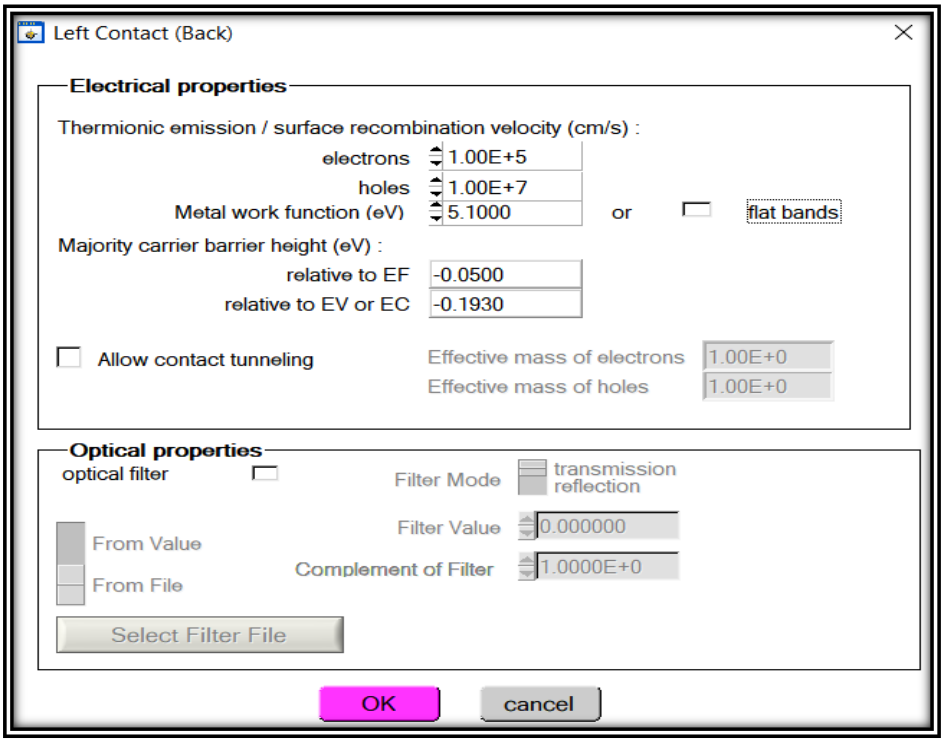

Figure 2.10: *Contact properties panel.*

f. Finally, once all the components have been added, and we have the necessary solar cell, we can save this structure by clicking the "Save" button, and we can now start the simulation by returning to the main interface (Figure 2.5) and clicking on "Calculate."

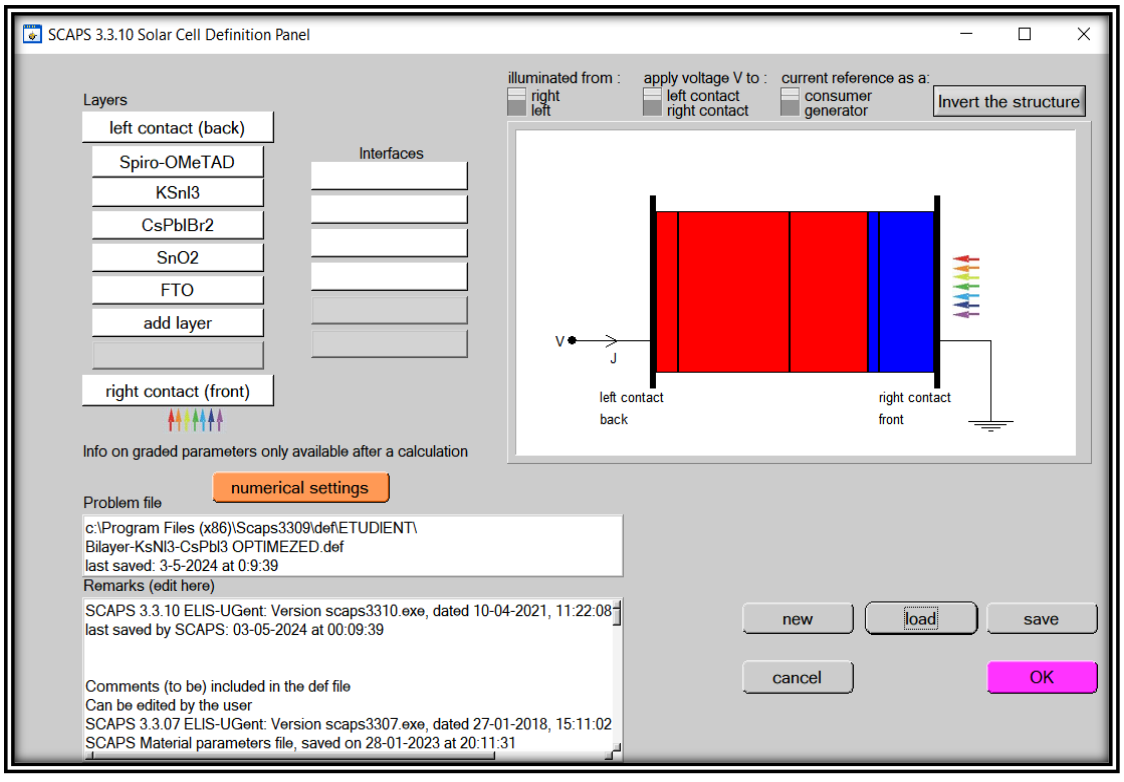

Figure 2.11: *Example of the simulation of our proposed $CsPbIBr_2/KSnI_3$ bilayer PSC structure.*

References Chapter 2 :

[1] Miyasaka, Tsutomu, et al. "Perovskite solar cells: can we go organic-free, lead-free, and dopant-free?." Advanced Energy Materials 10.13 (2020): 1902500.

[2] Kojima, Akihiro, et al. "Organometal halide perovskites as visible-light sensitizers for photovoltaic cells." Journal of the american chemical society 131.17 (2009): 6050-6051.

[3] Ma, Q., Chu, W., Wu, S., Wei, Q., Cheng, Z., Wu, J., ... & Dong, J. (2022). Design and performance optimization of carbon-based all-inorganic CsPbIBr2 perovskite battery with C60 buffer layer. Solar Energy, 246, 245-255.

[4] Scientific research and specialized studies in the field of solar cells

[5] D.S. Ginley, J.D. Perkins, Transparent conductors, in: Handbook of Transparent Conductors, Springer, 2011: pp. 1–25

[6] Moholkar, A. V., et al. "Effect of fluorine doping on highly transparent conductive spray deposited nanocrystalline tin oxide thin films." Applied Surface Science 255.23 (2009): 9358-9364.

[7] Mohammed, M. K., Al-Gazally, M. E., Khaleel, O. A., Al-Mousoi, A. K., Jeddoa, Z. M. A., Majdi, H. S., ... & Dastan, D. (2024). Improved eco-friendly CsSn 0.5 Ge 0.5 I 3 perovskite photovoltaic efficiency beyond 20% with SMe-TATPyr hole-transporting layer. *Physical Chemistry Chemical Physics*, *26*(4), 3229-3239.

[8] S.M. Sze, M.-K. Lee, Semiconductor Devices: Physics and Technology: Physics and Technology, Wiley Global Education, 2012.

[9] Khan, M. I., Mujtaba, A., Fatima, M., Marzouki, R., Hussain, S., & Anwar, T. (2024). Impact of Ce doping on the optoelectronic and structural properties of a CsPbIBr2 perovskite solar cell. Physical Chemistry Chemical Physics, 26(5), 4166-4173.

[10] Kumar, Mulmudi Hemant, et al. "Lead-free halide perovskite solar cells with high photocurrents realized through vacancy modulation." Advanced Materials (Deerfield Beach, Fla.) 26.41 (2014): 7122-7127.

[11] Ri, C. H., Kim, Y. S., Jong, U. G., Kye, Y. H., Ryang, S. H., & Yu, C. J. (2021). First-principles study on structural, electronic and optical properties of perovskite solid solutions KB 1− x Mg x I 3 (B= Ge, Sn) toward water splitting photocatalysis. RSC advances, 11(42), 26432-26443.

[12] Orthorhombic KSnI3. https://materialsproject.org/materials/mp-1097015/, 2022. (accessed august 08, 2024)

[13] Pindolia, G., Shinde, S. M., & Jha, P. K. (2023). Non-leaded, KSnI3 based perovskite solar cell: A DFT study along with SCAPS simulation. Materials Chemistry and Physics, 297, 127426.

[14] Kundara, R., & Baghel, S. (2024). Predictive design of KSnI3-based perovskite solar cells using SCAPS and machine learning model. Materials Science and Engineering: B, 307, 117536.

[16] Sheng, G., Zhao, Y., Zheng, J., Chen, L., Qiu, B., Zhong, L., ... & Xiao, X. (2023). Preannealing Process Improves the Efficiency of CsPbIBr2 Perovskite Solar Cells. Energy Technology, 11(1), 2200544.

[17] Khatoon, S., Chakraborty, V., Yadav, S. K., Diwakar, S., Singh, J., & Singh, R. B. (2023). Simulation study of CsPbIxBr1-x and MAPbI3 heterojunction solar cell using SCAPS-1D. Solar Energy, 254, 137-157.

[18] Li, S., Cao, Y. L., Li, W. H., & Bo, Z. S. (2021). A brief review of hole transporting materials commonly used in perovskite solar cells. Rare Metals, 40(10), 2712-2729.

[19] Hajjiah, A., Gamal, M., Kandas, I., Gorji, N. E., & Shehata, N. (2022). DFT and AMPS-1D simulation analysis of all-perovskite solar cells based on CsPbI3/FAPbI3 bilayer structure. Solar Energy Materials and Solar Cells, 248, 112026.

[20] Miyasaka, T., Kulkarni, A., Kim, G. M., Öz, S., & Jena, A. K. (2020). Perovskite solar cells: can we go organic-free, lead-free, and dopant-free?. Advanced Energy Materials, 10(13), 1902500.

[21] Burgelman, M., Nollet, P., & Degrave, S. (2000). Modelling polycrystalline semiconductor solar cells. Thin solid films, 361, 527-532.

[22] Pindolia, G., Shinde, S. M., & Jha, P. K. (2022). Optimization of an inorganic lead free RbGeI3 based perovskite solar cell by SCAPS-1D simulation. Solar Energy, 236, 802-821.

[23] Bencherif, H., Meddour, F., Elshorbagy, M. H., Hossain, M. K., Cuadrado, A., Abdi, M. A., ... & Alda, J. (2022). Performance enhancement of (FAPbI3) 1-x (MAPbBr3) x perovskite solar cell with an optimized design. Micro and Nanostructures, 171, 207403.

Chapter 3: Numerical simulation results and interpretation

3.1. Introduction

In this chapter, single and bilayer perovskite solar cells are investigated using 1-dimensional numerical simulations with the SCAPS simulator. Initially, a reference structure of FTO/SnO_2/$CsPbIBr_2$/Spiro/Au solar cell is simulated based on experimental data to validate the simulation and assess the extent to which the present results align with experimental data. However, the performance of a single perovskite absorber is limited. Therefore, we propose adding a new material as a bottom absorber layer to create the simulated cell structure FTO/SnO_2/$CsPbIBr_2$/$KSnI_3$/Spiro/Au. By comparing the simulation results of both single and bilayer perovskite structures, we demonstrate the effect of utilizing a bilayer on cell performance. Next, we optimize the bilayer PSC by adjusting various parameters such as thickness, density, doping, and temperature. Finally, we deduce the optimal structure for the $CsPbIBr_2$/$KSnI_3$ bilayer PSC structure.

3.2. Structures of PSCs and Simulation parameters used

Solar cells generally consist of several different layers, as shown in the perovskite cell in Figure 3.1.

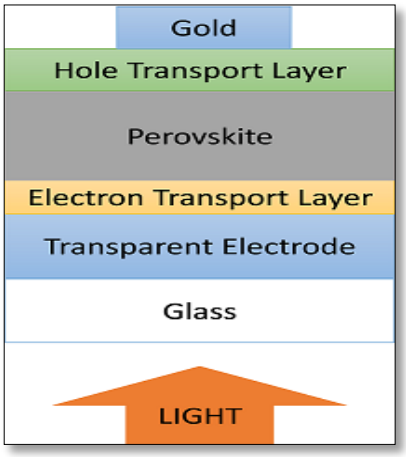

Figure 3.1: *The conventional structure of a perovskite solar cells.*

Typically, the perovskite cell is composed of many layers stacked on top of one another. The most crucial layers include:

- **Absorber Layer**

The absorber layer is the central part of the perovskite solar cell where light absorption occurs, generating electron-hole pairs. This layer is crucial as it determines the efficiency of light absorption and the subsequent generation of charge carriers, which are then transported to the ETL and HTL.

- **Electron Transport Layer (ETL)**

The primary roles of the electron transport layer (ETL) in a solar cell are to promote the movement of electrons from the active layer to the electrode and to obstruct the movement of holes to the electrode. By lowering energy loss and speeding up charge transfer, this layer helps to increase cell efficiency [4].

- **Hole Transport Layer (HTL)**

The Hole Transport Layer (HTL) in a solar cell is a layer used to transfer holes from the active layer to the electrode, preventing electrons from being transferred to the electrode. This layer contributes to improving cell efficiency by facilitating charge transfer and reducing energy loss [4].

- **Transparent and metallic electrode**

In solar cells, transparent electrodes like indium tin oxide (ITO) or fluorine-doped tin oxide (FTO) allow light to reach the active layers while conducting electrical current. Metallic electrodes, such as gold or aluminum, are used as back contacts for their superior conductivity, aiding in efficient charge collection [5,6].

In this study, our aim was to understand the operation of $CsPbIBr_2/KSnI_3$ bilayer PSCs. To do this, we first simulated the performance of a single-junction $CsPbIBr_2$-based PSC. We then analyzed the performance of a $CsPbIBr_2/KSnI_3$ bilayer PSC. By comparing the results from these two configurations, we can evaluate and clarify the impact and importance of utilization of using two absorber layers within the device. Figures 3.2 (a) and (b) illustrate the schematic structures of the single-junction $CsPbIBr_2$ PSC and the $CsPbIBr_2/KSnI_3$ bilayer PSC, respectively.

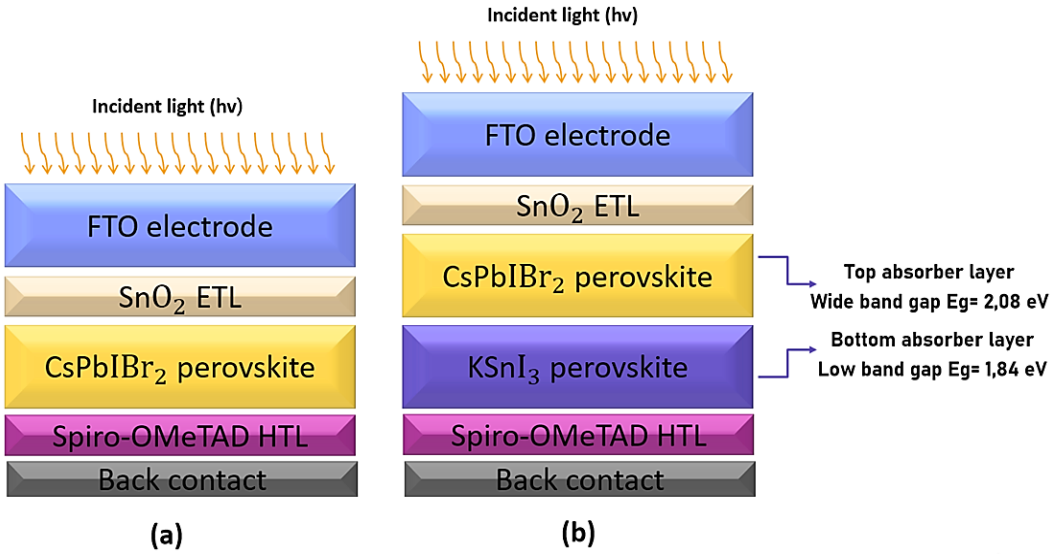

Figure 3.2: *Configuration of (a) Single-Junction and (b) Bilayer PSCs.*

Both cells feature an FTO layer as the front contact and a gold (Au) layer as the metal back contact. The electron transport layer (ETL) is made of SnO_2, while the hole transport layer (HTL) is composed of Spiro-OMeTAD. The main difference between the two structures is in the absorber layer configuration. In structure (a), $CsPbIBr_2$ is solely used as the absorber layer. In contrast, structure (b) employs a heterojunction with $CsPbIBr_2$ and $KSnI_3$ as the absorber layers, with $CsPbIBr_2$ as the top layer and $KSnI_3$ as the bottom layer.

The parameters for calculating the cell structures are detailed in Table 3.1. The simulation was conducted under incident irradiation of 1000 W/m² and at an operating temperature of 300 K.

Table 3.1: Parameters of devices utilized in the simulation [7-12].

Parameters	Layers				
	FTO	SnO_2	$CsPbIBr_2$	$KSnI_3$	Spiro
Bandgap, E_g (eV)	3.5	3.5	2.08	1.84	2.85
Electron affinity, χ_e (eV)	4	4	3.7	3.44	2.2
Dielectric ratio, E_{ps}	9	9	8	10.4	3
Electron mobility, μ_n (cm^2/Vs)	20	20	20	21.28	2.1×10^{-3}
Hole mobility, μ_p (cm^2/Vs)	10	10	20	19.46	2.6×10^{-3}
Valence band density of states, N_v (cm^{-3})	1.8×10^{19}	1.8×10^{19}	5×10^{18}	1.8×10^{19}	2.5×10^{20}
Conduction band density of states, N_c (cm^{-3})	2.2×10^{18}	2.2×10^{18}	2×10^{18}	2.8×10^{18}	2.5×10^{20}
Donor concentration, N_d (cm^{-3})	1×10^{19}	1×10^{17}	-	1×10^{15}	-
Acceptor concentration, N_a (cm^{-3})	-	-	1×10^{15}	1×10^{15}	1×10^{18}
Defect Density, N_t (cm^{-3})	1×10^{15}	1×10^{15}	1×10^{14}	1×10^{14}	1×10^{15}

3.3.Simulation results

At the start of this numerical simulation, we first simulate a single-junction $CsPbIBr_2$ PSC, followed by a $CsPbIBr_2/KSnI_3$ bilayer PSC, as illustrated in Figure 3.2.

Figures 3.3 and 3.4 present the initial simulation outcomes for a single-junction $CsPbIBr_2$-based device and a $CsPbIBr_2/KSnI_3$ bilayer device. In addition, Table 3.3 summarizes the characteristics of a single-junction $CsPbIBr_2$-based device, as extracted from Figure 3.3. The good agreement between the simulation and experimental results indicates that the simulation process is accurate.

Table 3.2: Photovoltaic output parameters of $CsPbIBr_2$ Single-Junction and $CsPbIBr_2/KSnI_3$ Bilayer PSC

Device configuration	J_{sc} (mA/cm^2)	V_{oc}(V)	*FF* (%)	*PCE* (%)
FTO/SnO_2/ $CsPbIBr_2$/ Spiro/Au	8.80	1.69	65.11	9.70
FTO/SnO_2/$CsPbIBr_2$/$KSnI_3$/ Spiro/Au	14.69	1.45	78.28	16.90

A comparison of the J-V curves for these two structures, as depicted in Figure 3.3, clearly indicates that the bilayer PSC structure surpasses the performance of the single-junction PSC structure. Additionally, as illustrated in Figure 3.4, the $CsPbIBr_2/KSnI_3$ bilayer PSC exhibits the

widest light absorption range. This broader absorption range is the reason for the higher PCE of the $CsPbIBr_2/KSnI_3$ bilayer PSC compared to the single-junction PSC, which is mainly due to the bottom absorber layer $KSnI_3$, which has a suitable band gap of 1.84 eV. In more detail, as shown in Table 3.2, the $CsPbIBr_2/KSnI_3$ PSC achieves a PCE of 16.90%, while the $CsPbIBr_2$ single-junction PSC reaches only a PCE of 9.70%. These results suggest that using two absorber layers is an effective strategy for enhancing PSC performance, with $KSnI_3$ proving to be a highly suitable choice for the bottom absorber layer.

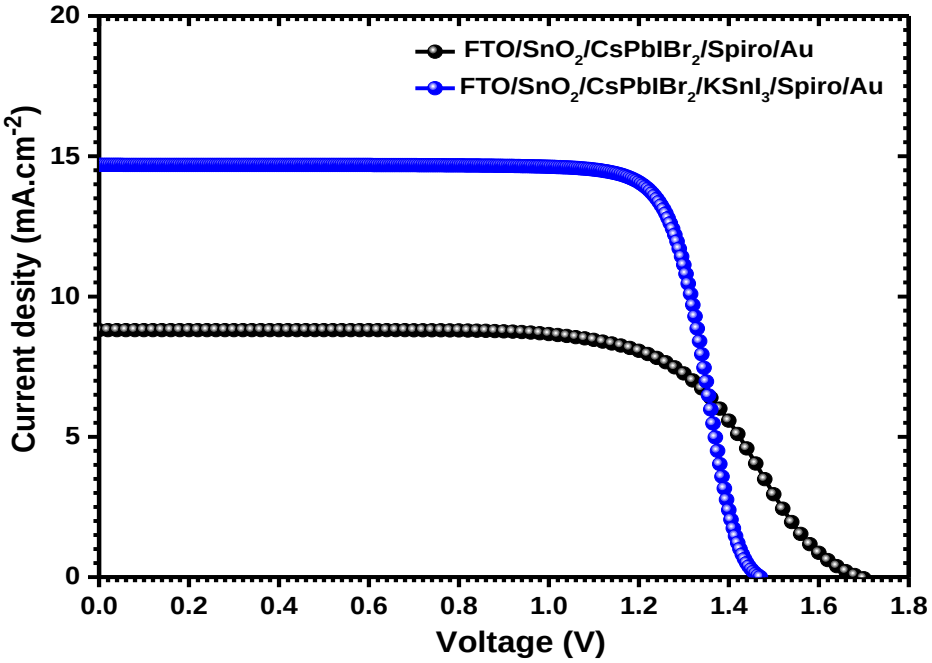

Figure 3.3: *Comparison of the J-V Characteristics between CsPbIBr2 Single-Junction and $CsPbIBr_2/KSnI_3$ Bilayer PSCs.*

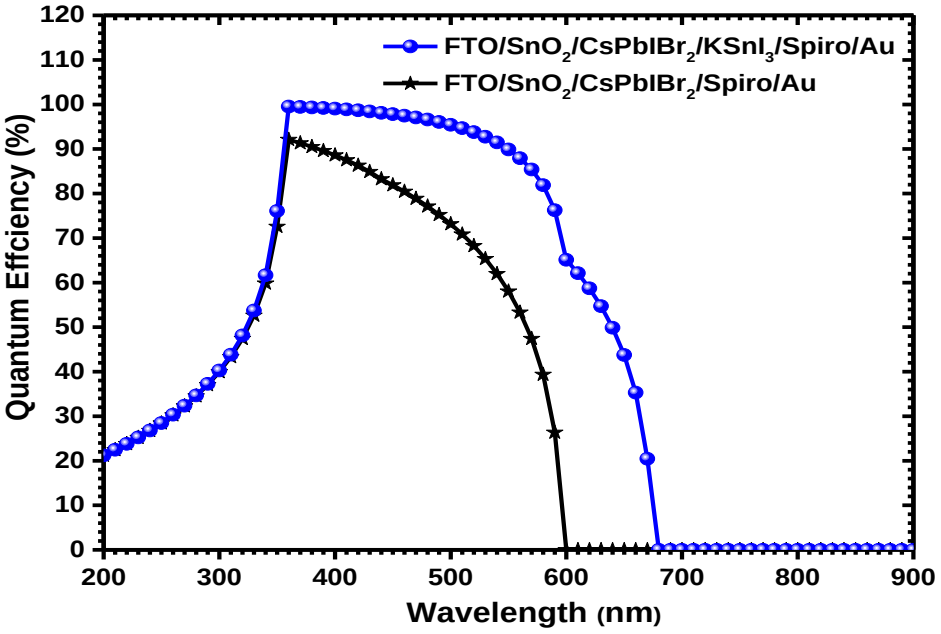

Figure 3.4: *Comparison of the Quantum efficiency Characteristics between CsPbIBr2 Single-Junction and $CsPbIBr_2$/ $KSnI_3$ Bilayer PSCs.*

Table 3.3: Results of our work compared to previous experimental results.

Device configuration	J_{sc} (mA/cm^2)	V_{oc}(V)	*FF* (%)	*PCE* (%)
FTO/TiO_2/ $CsPbIBr_2$/ Spiro/Au (Experimental) [1]	11.51	1.12	74	9.71
ITO/ SnO_2/C_{60}/ $CsPbIBr_2$/ Spiro/Au (Experimental) [2]	8.32	1.18	74.80	7.34
FTO/SnO_2/ $CsPbIBr_2$/ Spiro/Au (Experimental) [3]	10.79	1.24	71.68	9.60
FTO/SnO_2/ $CsPbIBr_2$/ Spiro/Au (This work)	8.80	1.69	65.11	9.70

3.3.1. Optimization of bilayer PSC

3.3.1.1. Effect of $CsPbIBr_2$ top absorber layer on bilayer PSC Performance

We initially simulated the performance of the bilayer PSC by varying the thickness of the $CsPbIBr_2$ top absorber layer between 100 nm and 2000 nm to assess its impact on the device's performance. Figure 3.5 shows the bilayer PSC performance with varying $CsPbIBr_2$ top absorber layer thickness. As the thickness of $CsPbIBr_2$ increases, efficiency also increases, reaching a peak of 17.08% at 700 nm. Beyond this point, further increases in thickness result in a gradual decrease in efficiency. Therefore, a thickness of 700 nm was chosen as the optimal thickness for the $CsPbIBr_2$ top absorber layer for the remainder of this study.

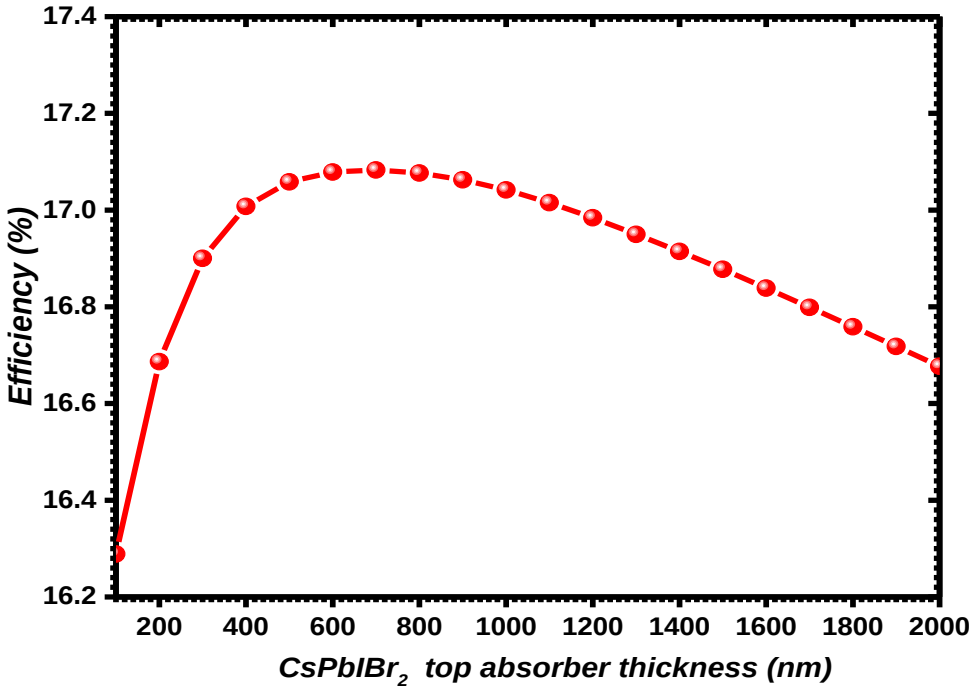

Figure 3.5: *Efficiency change curve as a function of $CsPbIBr_2$ thickness.*

3.3.1.2. Effect of $KSnI_3$ bottom absorber layer on bilayer PSC Performance

After setting the thickness of the $CsPbIBr_2$ top absorber layer to 700 nm, the next step is to examine the effect of the $KSnI_3$ bottom absorber layer in terms of thickness, acceptor density, and donor density on the cell's efficiency. Figure 3.6 shows the efficiency curve as a function of the $KSnI_3$ bottom absorber layer thickness, ranging from 100 to 2000 nm. It is evident that the

efficiency increases rapidly with increasing thickness, reaching a peak at 1000 nm with a maximum efficiency of 18.52%, before gradually decreasing as the thickness continues to rise.

Subsequently, we fixed the thickness of $KSnI_3$ at 1000 nm and varied the acceptor density from 1×10^{12} to 1×10^{18} cm^{-3}, as shown in Figure 3.7. It can be observed that when the density surpasses $N_A(KSnI_3) = 1 \times 10^{15}$ cm^{-3}, the efficiency increases rapidly, reaching a value of 21.87% at $N_A(KSnI_3) = 1 \times 10^{18}$ cm^{-3}.

Next, we fixed the $KSnI_3$ acceptor density at $N_A(KSnI_3) = 1 \times 10^{16}$ cm^{-3} and varied the donor density from 1×10^{12} to 1×10^{16} cm^{-3}. Figure 3.8 shows that the efficiency remains almost constant until $N_D(KSnI_3)$ exceeds 10^{16} cm^{-3}, after which it gradually decreases.

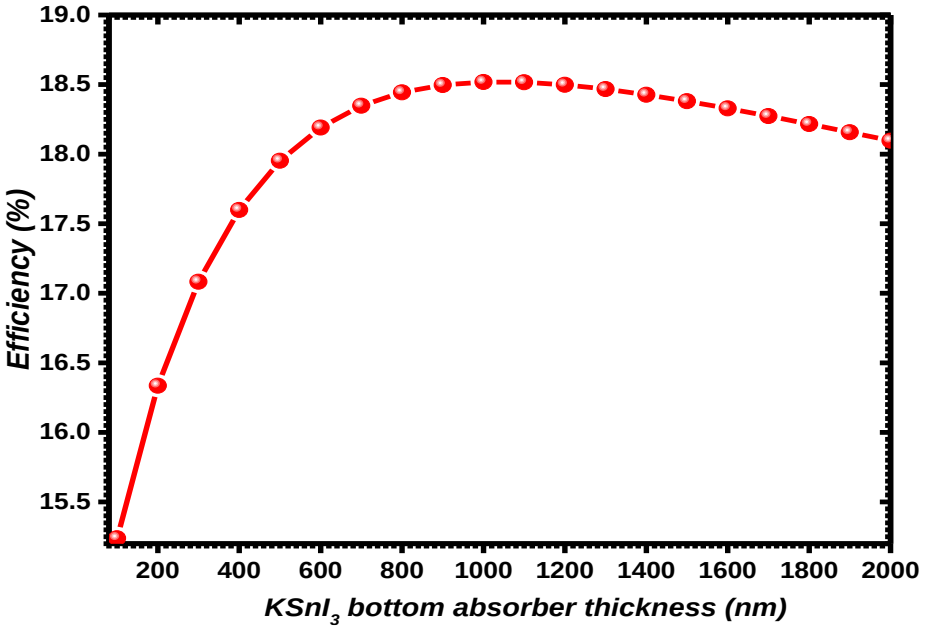

Figure 3.6: *Efficiency change curve as a function of $KSnI_3$ thickness.*

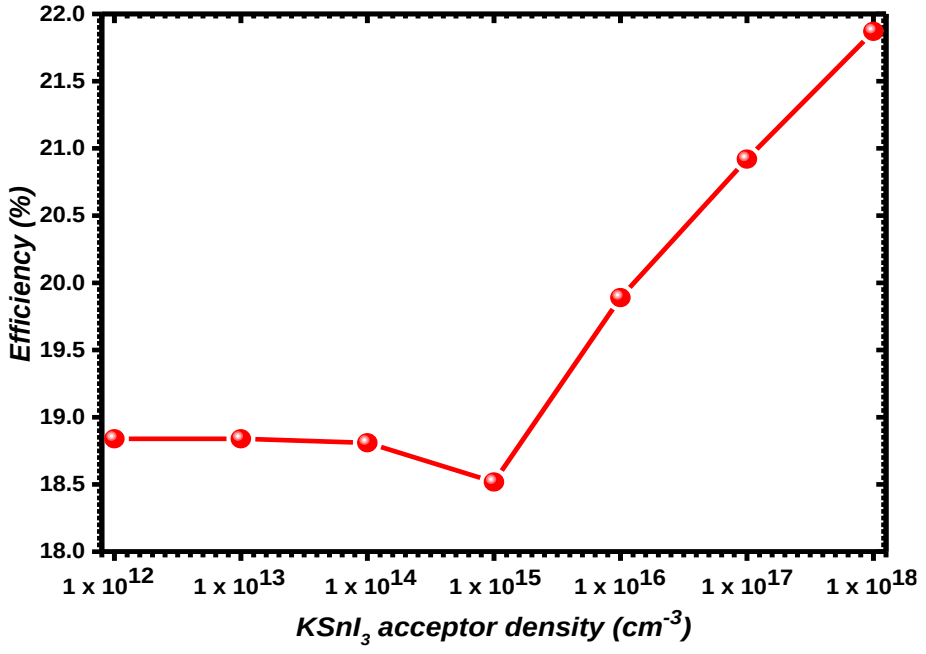

Figure 3.7: *Efficiency change curve as a function of $KSnI_3$ acceptor density.*

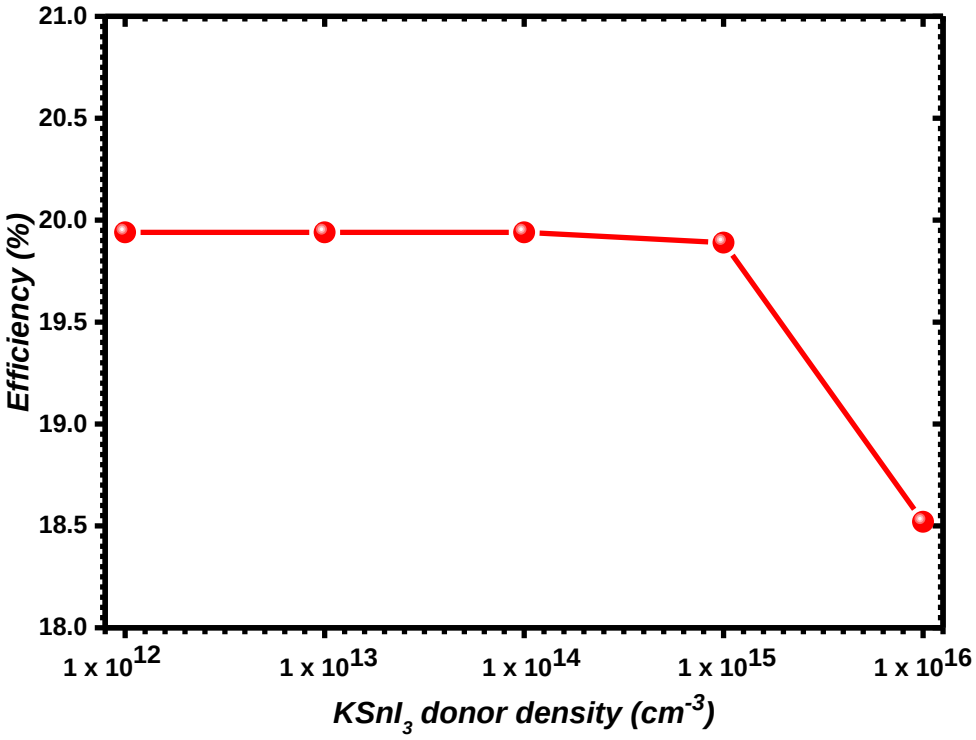

Figure 3.8: *Efficiency change curve as a function of $KSnI_3$ donor density.*

Therefore, based on the previous figures, we deduce that:

- From Figure 3.6, the optimum thickness of the $KSnI_3$ bottom absorber layer is 1000 nm.
- According to Figures 3.7 and 3.8, the appropriate values for the acceptor density and donor density are approximately $N_A(KSnI_3) = 1 \times 10^{16}$ cm^{-3} and $N_D(KSnI_3) = 1 \times 10^{15}$ cm^{-3}, respectively. These parameters are selected because they align well with previously published results in the literature [7].

3.3.1.3. Effect temperature on bilayer PSC Performance

Temperature is another crucial factor that significantly impacts cell efficiency. The previous results were all obtained at a constant temperature of 300 K. To explore and understand the stability of the optimized bilayer PSCs, the effect of temperature variations ranging from 260 to 350 K on performance was examined, with the resulting efficiency changes shown in Figure 3.9.

We observe that efficiency initially increases from 260 K to 330 K, then gradually decreases as the temperature rises above 330 K. Therefore, from the curve, it can be concluded that the optimal efficiency is achieved within a temperature range of 310 to 330 K.

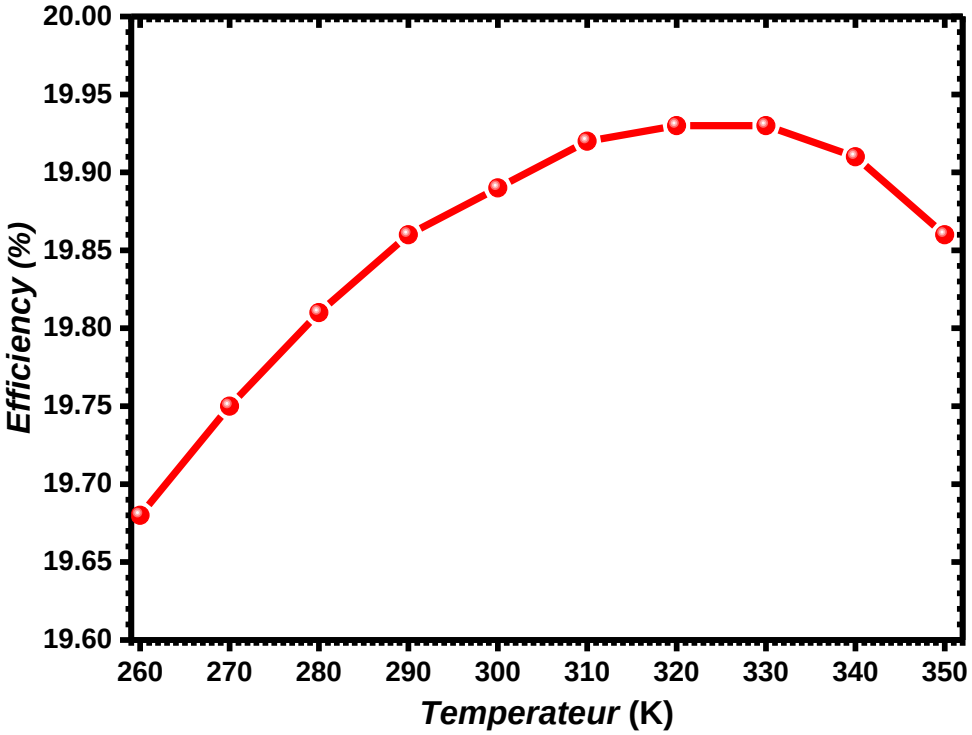

Figure 3.9: *Efficiency change curve as a function of temperature.*

3.3.2. Optimum design

In the end, we found that the efficiency of the solar cell increased after the previous improvement process, as shown in Figures 3.10 and 3.11, compared to the bilayer cell before the improvement. The optimal design, based on the optimal thickness and acceptor doping density of the $CsPbIBr_2$ layer, was determined to be 700 nm and $N_A = 1\times10^{19}$ cm^{-3}, respectively, with a fixed optimal thickness and acceptor doping density of $KSnI_3$ at 1000 nm and $N_A = 1\times10^{16}$ cm^{-3}. Table 3.4 summarizes the performance characteristics of the single-layer and bilayer cells, indicating an optimum efficiency of 19.89% for the optimized bilayer PSC.

Table 3.4: Photovoltaic output parameters of $CsPbIBr_2$ Single-Junction and $CsPbIBr_2$/ $KSnI_3$ (before and after optimization).

Device configuration	J_{sc} (mA/cm^2)	V_{oc}(V)	*FF* (%)	*PCE* (%)
FTO/SnO_2/ $CsPbIBr_2$/ Spiro/Au	8.80	1.69	65.11	9.70
FTO/SnO_2/$CsPbIBr_2$/$KSnI_3$/ Spiro/Au	14.69	1.45	78.28	16.90
FTO/SnO_2/$CsPbIBr_2$/$KSnI_3$/ Spiro/Au (optimized)	17.70	1.43	78.50	19.89

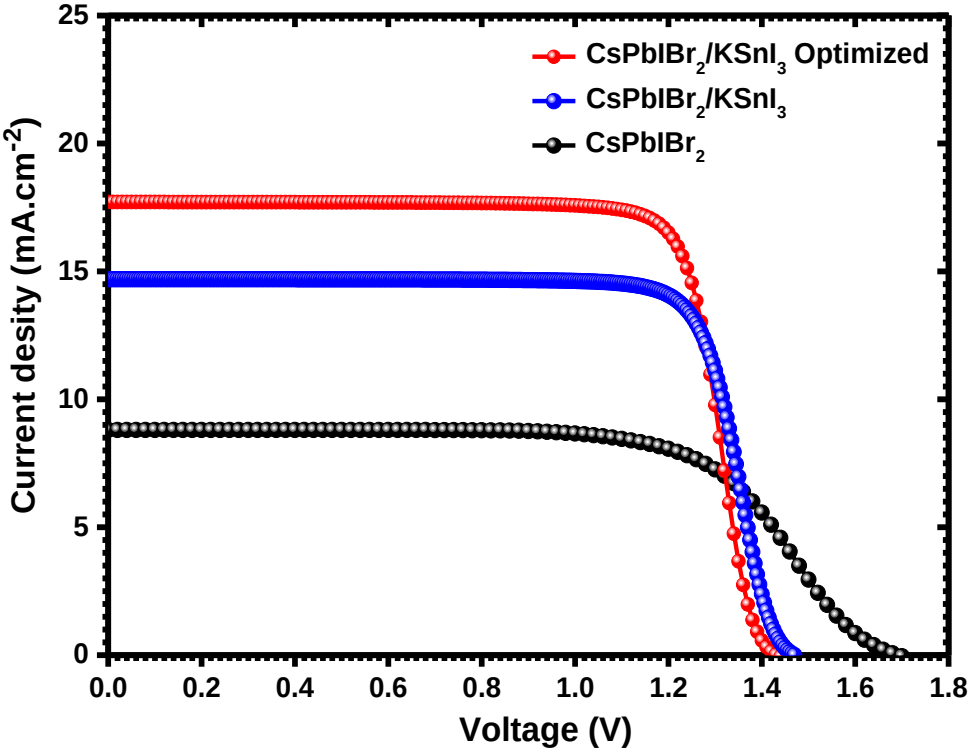

Figure 3.10: *Comparison of the J-V Characteristics of Single-Junction and Bilayer PSCs (before and after optimization).*

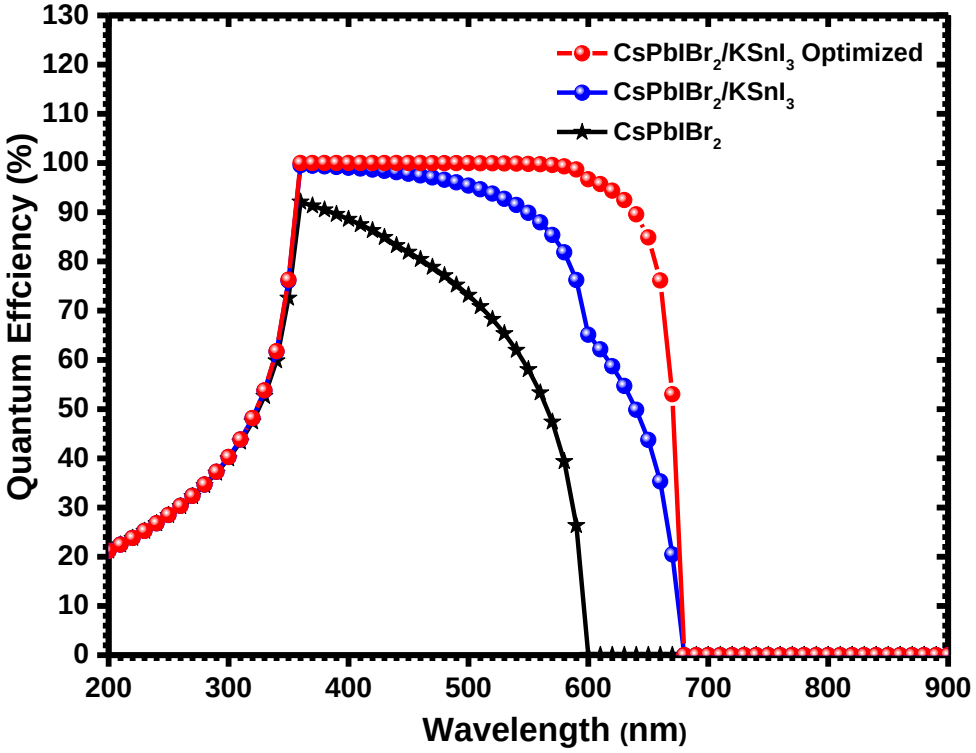

Figure 3.11: *Comparison of the Quantum efficiency Characteristics of Single-Junction and Bilayer PSCs (before and after optimization).*

References Chapter 3:

[1] Khan, M. I., Mujtaba, A., Fatima, M., Marzouki, R., Hussain, S., & Anwar, T. (2024). Impact of Ce doping on the optoelectronic and structural properties of a CsPbIBr2 perovskite solar cell. Physical Chemistry Chemical Physics, 26(5), 4166-4173.

[2] Li, N., Zhu, Z., Li, J., Jen, A. K. Y., & Wang, L. (2018). Inorganic CsPb1− xSnxIBr2 for efficient wide-bandgap perovskite solar cells. Advanced energy materials, 8(22), 1800525.

[3] Sheng, G., Zhao, Y., Zheng, J., Chen, L., Qiu, B., Zhong, L., ... & Xiao, X. (2023). Preannealing Process Improves the Efficiency of CsPbIBr2 Perovskite Solar Cells. Energy Technology, 11(1), 2200544.

[4] Li, Dong, et al. "Investigating Ultrafast Electron Transfer in Graphene and Its Derivatives Composites by Femtosecond Transient Absorption Spectroscopy." ChemPhotoChem (2024): e202300271.

[5] Counter Electrode Material Selection for Dye-Sensitized Solar Cells: A Review" ،C. Karunakaran Journal of Materials Science: Materials in Electronics ،2017.

[6] Sheehan, S., et al. "Flexible glass substrate based dye sensitized solar cells." Solar Energy Materials and Solar Cells 132 (2015): 237-244.

[7] Pindolia, G., Shinde, S. M., & Jha, P. K. (2023). Non-leaded, KSnI3 based perovskite solar cell: A DFT study along with SCAPS simulation. Materials Chemistry and Physics, 297, 127426.

[8] Khatoon, S., Chakraborty, V., Yadav, S. K., Diwakar, S., Singh, J., & Singh, R. B. (2023). Simulation study of CsPbIxBr1-x and MAPbI3 heterojunction solar cell using SCAPS-1D. Solar Energy, 254, 137-157.

[9] Ma, Q., Chu, W., Wu, S., Wei, Q., Cheng, Z., Wu, J., ... & Dong, J. (2022). Design and performance optimization of carbon-based all-inorganic CsPbIBr2 perovskite battery with C60 buffer layer. Solar Energy, 246, 245-255.

[10] Hajjiah, A., Gamal, M., Kandas, I., Gorji, N. E., & Shehata, N. (2022). DFT and AMPS-1D simulation analysis of all-perovskite solar cells based on CsPbI3/FAPbI3 bilayer structure. Solar Energy Materials and Solar Cells, 248, 112026.

[11] Bencherif, H., Meddour, F., Elshorbagy, M. H., Hossain, M. K., Cuadrado, A., Abdi, M. A., ... & Alda, J. (2022). Performance enhancement of (FAPbI3) 1-x (MAPbBr3) x perovskite solar cell with an optimized design. Micro and Nanostructures, 171, 207403.

[12] Pindolia, G., Shinde, S. M., & Jha, P. K. (2022). Optimization of an inorganic lead free RbGeI3 based perovskite solar cell by SCAPS-1D simulation. Solar Energy, 236, 802-821.

General conclusion

General Conclusion

In conclusion, this study investigated single absorber layer solar cells composed of $CsPbIBr_2$, as well as the incorporation of $KSnI_3$ Perovskite to create bilayer absorber Perovskite solar cells using the SCAPS-1D simulator. The results demonstrated that $CsPbIBr_2$/ $KSnI_3$ bilayer PSCs exhibit superior performance compared to single absorber solar cells. The bilayer PSCs show a broadened absorption spectrum, which enhances the overall device performance. By optimizing the thickness of the absorber layers and the density of the donor and acceptor, we were able to significantly increase the efficiency of bilayer PSCs. The results revealed that the efficiency of bilayer PSCs improved with these optimizations, achieving the best performance with a bottom absorber $KSnI_3$ thickness of 1000 nm, a donor density of 1×10^{15} cm^{-3}, and an acceptor density of 1×10^{16} cm^{-3}, combined with a top absorber $CsPbIBr_2$ thickness of 700 nm. Furthermore, the optimal operating temperature for these solar cells was found to be between 300 and 320 K. These results highlight the great potential to improve the efficiency of solar cells through modifications in design and materials used. As we continue to improve these factors, we can achieve greater performance improvements and advances in the use of solar energy as a clean and efficient energy source.

Ultimately, we hope that this study will contribute to the development of new technologies in the field of solar cells and stimulate more research and innovations to achieve higher efficiency and greater sustainability in the future.